Interacting Multiple Model Filtering for Aircraft Guidance Modes Identification from Surveillance Data

Homeyra Khaledian*
Technical University of Catalonia (UPC), 08860, Castelldefels, Spain.

Raúl Sáez†
Technical University of Catalonia (UPC), 08860, Castelldefels, Spain.
International Centre for Numerical Methods in Engineering (CIMNE), 08034, Barcelona, Spain.

Jordi Vilà-Valls ‡
University of Toulouse, 31055, Toulouse, France.

Xavier Prats §
Technical University of Catalonia (UPC), 08860, Castelldefels, Spain.

Accurate and reliable trajectory prediction (TP) is required in several air traffic management systems. Estimating the aircraft trajectory in a vertical plane typically requires the knowledge of a pair of operational instructions. A sequence of operational instructions specify the aircraft intent, information which is seldom available, besides for the ownship trajectory planning system. In the execution of the trajectory, the aircraft is directed by the (auto)pilot through a series of sequential guidance modes that might override some of the planning instructions of the aircraft intent. Therefore, having reliable guidance mode information is fundamental for next generation of air- or ground-based TP. The main goal of this contribution is to develop a methodology able to identify in real-time the active guidance modes for both vertical climb and descent profiles, using only Automatic Dependent Surveillance-Broadcast and Enhanced Mode-S Surveillance data. The proposed solution is based on an interacting multiple model (IMM) filtering approach, which uses a bank of filters, each one matched to a possible guidance mode. The guidance mode identification performance of the IMM-based solution is validated with: i) a set of simulated representative trajectories and ii) real flight data obtained from flight data recorders.

*PhD candidate, Department of Physics-Aerospace Division, Esteve Terradas, 5, Building C3C, Office 121.

†Post-doctoral researcher, Department of Physics-Aerospace Division at UPC and Aeronautics Group in CIMNE, Esteve Terradas, 5, Building C3C, Office 121.

‡Professor, Institut Supérieur de l'Aéronautique et de l'Espace (ISAE-SUPAERO); Jordi.vila-valls@isae-supaero.fr (Corresponding Author).

§*Serra i Hunter* fellow (associate professor), Department of Physics-Aerospace Division, Esteve Terradas, 5, Building C3C, Office 104.

I. Introduction

Single European Sky Air Traffic Management (ATM) Research (SESAR) and the United States' Next Generation Air Transportation System (NextGen) are among the first ATM modernization programs* that conceptualize the recent advances in avionics technology and ATM systems [1]. Both programs share common goals built on the notion of trajectory-based operations (TBO), in contrast to the current airspace-centric paradigm. Both programs attempt to dynamically manage flights on an end-to-end time basis as cost-efficiently as possible, enabling airspace users to fly their preferred flight trajectories [2]. Within the TBO paradigm, stakeholders will actively participate in the exchange, maintenance, and use of consistent aircraft trajectories and flight information data. In the TBO context, aircraft trajectory prediction (TP) algorithms will play an important role.

During the execution of a flight—the focus of this contribution—TP is (or will be) present in advanced on-board trajectory planning and guidance algorithms (for *ownship* trajectories); in applications to enable, for instance, self-separation or conformance monitoring (i.e., predicting *intruder* trajectories) [3]; and in a plethora of ground-based air traffic control (ATC) decision support tools, such as for separation management or aircraft sequencing and merging purposes in terminal airspace [4]. Furthermore, advanced TP capabilities are also a key enabler for safety nets, advisory or warning tools, either for on-board or ground-based collision warning and avoidance systems. The reader could refer, for instance, to [5, 6] for reviews on TP and collision detection and resolution algorithms (CDR).

In practice, TP algorithms estimate the most likely four-dimensional (4D) trajectory of an aircraft given its observed current state (i.e., initial conditions); a weather forecast (which could be available from a numerical weather prediction model†); an aircraft performance model (APM); a set of operational constraints; and the aircraft intent [8]. Aircraft intent contains all the information needed to unambiguously describe and compute the trajectory and it is composed by a set of operational instructions which "*capture a basic command, guidance mode or control strategy at the disposal of the pilot/flight management system (FMS) to direct the operation of the aircraft. They are the trajectory atomics or primitives into which every trajectory could be decomposed*" [9].

When the trajectory is finally executed, however, the (auto)pilot is responsible to steer the aircraft using a sequence of specific guidance modes to follow (as much as possible) the planned trajectory. For instance, in a vertical plane, aircraft have two independent actuators: elevator and engine throttle. Among all different planned variables that define a 4D trajectory, the guidance function of the FMS chooses which two variables the (auto)pilot should follow (or track) with these two actuators. Then, if the models used to plan the reference trajectory are good enough, the guidance system will typically command the aircraft actuators to follow the instructions that define the aircraft intent that was initially planned. In a real flight, however, the guidance function might switch to different guidance modes in order to prevent deviating too much from the reference trajectory plan, as deviations will occur due to uncertainty in the models, sensors,

*Similar initiatives have been launched in Asia-Pacific countries, e.g., OneSky (Australia), the collaborative actions for renovation of air traffic systems (Japan) and the ATM Bureau Strategic Development Program (China).

†In addition, sharing ownship measured meteorological data with surrounding aircraft could also lead to enhanced on-board TP capabilities [7].

actuators response times, etc.; respect the flight envelope; and operate the actuators within their limits. Therefore, the execution of the planned trajectory leads to the application of a sequence of guidance modes that ultimately steer the aircraft.

Aircraft intent uncertainty is defined as the difference between the initially planned instructions of the aircraft intent and the guidance modes finally executed by the (auto)pilot [8]. Hence, in order to predict a trajectory while it is being executed, it will be necessary to predict the guidance modes that are being used by the guidance system of the aircraft, not the instructions that were used at the planning stage. Uncertainty of the aircraft intent instructions may impact the prediction performance, a problem that can be mitigated with guidance mode identification capabilities (as proposed in this article), which in turn may boost the overall trajectory prediction accuracy. Reliable guidance information is especially critical in the vertical domain of the trajectory, since slight input inaccuracies or an incorrect guidance mode identification easily propagate along the predicted trajectory. This may lead to large discrepancies in the predicted altitude, speed, estimated times of arrival, fuel consumption, etc. Indeed, an incorrect guidance modes estimation can also jeopardize efforts devoted to obtain accurate aircraft performance and weather models [8, 10]. Then, for a plethora of applications relying on various kinds of TP, guidance mode identification/estimation is fundamental as it may drive the overall TP performance.

Several TP approaches are available in the literature, which can be mainly divided into machine learning-based (ML) techniques and stochastic methods. A comprehensive survey of the former is given in [11]. While ML-based approaches may be interesting if large data sets are available [12–14], they also have several limitations: i) a lack of system understanding, ii) it is not possible to theoretically assess performance limits, iii) the knowledge of physical parametric models is disregarded, and iv) for safety-critical applications it is unlikely that they could be certified. To the best of the authors' knowledge, such techniques have not been yet applied to guidance mode identification, and are out of the scope of this article. A different approach is to rely on stochastic methods, which rather than learning the system from data, exploit the physical knowledge of the TP problem at hand. Such physical modelling can be expressed for instance in state-space form, including: i) the dynamic aircraft model (e.g., a point-mass model); ii) the available data [15–19]. For instance, Automatic Dependent Surveillance-Broadcast (ADS-B), Enhanced Mode-S Surveillance (EHS), aircraft surveillance data, or extended projected profile (EPP); and iii) the system uncertainty, which has been studied in detail [8, 20]. In this case, TP becomes an estimation problem. For instance, [21] proposed an adaptive algorithm that dynamically adjusts the modeled aircraft weight based on observed radar track data to improve the climbing phase TP accuracy. In [22], a probabilistic approach combined the aircraft dynamics (changing flight modes) with flight intent information to provide a reliable 4D TP and conflict detection.

In the case where several dynamic system models appear (e.g., guidance modes), one can resort to multiple model (MM) techniques such as the interacting MM (IMM) filter [23]. In [24], a MM filter, based on 2D kinematic models, was used to improve aircraft tracking for CDR applications. Similarly, in [25] a MM filter was developed to identify

aircraft maneuvers during taxi operations. An enhanced MM filter using a nonlinear point-mass model to describe 3D aircraft dynamics was proposed in [26], showing significant benefits in terms of position estimation accuracy and filter robustness with respect to conventional kinematic-based filters. All these works, however, aim at identifying simple maneuvers in the horizontal plane, such as coordinated turns, constant speed or acceleration segments, thus, not being suited for the TP problem at hand. In [27, 28], maneuvers in the vertical plane were considered, but the algorithm was limited to identify simple maneuvers such as constant rate of climb/descent at constant speed. These limitations were partially addressed in [29], where a set of guidance modes for a typical aircraft descent were taken into account. All these promising results showed that IMM-based solutions are a powerful tool for TP, which still needs to be statistically characterized and tested for a comprehensive set of climb and descent trajectories.

The main goal of this contribution is to develop a methodology able to identify in real-time the active guidance modes in the vertical trajectory domain, for both climbs and descents, observing only ADS-B and EHS aircraft surveillance data. The proposed approach is based on the IMM filter [23, 30], a well-known recursive estimation method. IMM is able to tackle with systems that can contain several modes of operation, that is, when the dynamic system may be described by different state-space models. Besides the guidance mode—taken as the most likely model determined by the filter—the IMM also provides aircraft state estimation.

A key step is to know the optimal achievable performance of the filter, i.e., how well it can estimate both the state of the system (aircraft trajectory) and the guidance modes (the final and ultimate goal). Then, one wants to minimize the error between the estimated parameters and the true ones or, in terms of guidance modes, maximize the percentage of time that the true mode is identified. By optimal (from an estimation theory standpoint), we refer to the performance given by a filter in the mean square error sense under nominal conditions, i.e., when the problem is fully under control, without any unknown additional disturbance affecting the system, in the ideal case where the measurement and process noise distributions (and parameters), as well as the guidance command parameters are known. In this study, such characterizations are taken into account to give a performance benchmark that can be achieved by using synthetic data. Nevertheless, using real data, we would no longer be under nominal conditions, and the optimal performance of the filter requires such characterization to cope with real-life conditions.

Even if some works already used MM filtering techniques to estimate aircraft maneuvers [24–29], a comprehensive IMM-based guidance mode identification and performance statistical analysis, addressing the set of complex guidance modes that describe aircraft vertical dynamics for both climbs and descents, is not available in the literature to the best of the author's knowledge. Therefore, for the proposed IMM-based methodology the following points are addressed:

- Statistical analysis to assess the method performance under nominal conditions, for both climbs and descents.
- The most challenging part of the trajectory from an estimation point of view, that is, descent and climb trajectories at lower altitudes are analyzed, for non-clean (refers to the case that high-lift devices and landing gear are not deployed) aircraft configurations with high-lift devices and landing gear deployment.

- The method is also validated with real flight data obtained from flight data recorders (FDR).

II. Aircraft Trajectory Planning and Execution

Modern aircraft have high levels of flight automation, mostly implemented in what is commonly called FMS[‡] [9, 31–33]. Among other functionalities, the FMS is in charge of planning a trajectory, then, of supporting the (automatic) execution of the trajectory, providing guidance commands to the autopilot or to the flight director if the aircraft is manually flown. The trajectory plan is decomposed into a lateral route, following a sequence of waypoints, and a vertical profile, i.e., time histories of pressure altitude and speed, typically given in terms of Mach number or calibrated airspeed (CAS). This article focuses only on vertical profiles.

Before take-off, the FMS generates the most cost-efficient trajectory plan, according to some flight intent and that complies with all operational and flight envelope constraints. Similarly, the FMS generates a new and unique trajectory plan in cruise, before starting the descent; or at any point if manually triggered by the pilot. Planned trajectories have to be materialized or executed in flight. For this purpose, the FMS has a variety of guidance modes and functionalities to follow the plan and to react in different ways in case deviations from the plan occur. This section describes the mathematical process that underpins the computation (planning) and execution (guidance) of realistic trajectories for typical airliners.

A. Trajectory Planning and Simulation

Mathematically speaking, the motion of an aircraft can be described by a system of ordinary differential equations (ODEs), derived from the combination of translational (force) and rotational (moment) equations of movement. Although this six degrees of freedom (6DoF) model results in the most accurate planning of an aircraft trajectory, it requires an extensive aerodynamic and propulsive model and the knowledge of the inertia tensor of the aircraft. In the FMS, the aircraft rotational rate is small enough to consider only the translational equations of movement, leading to a three degrees of freedom (3DoF) model [34], which is sufficient for trajectory planning purposes. Some ATM applications use even simpler models, such as total energy or pure kinematic models [35]. It is worth noting that FMS are commercial devices subject to intellectual property rights and the exact models used and implementation details are not publicly disclosed. Depending on the FMS manufacturer, different aircraft motion models, APM, and/or weather models might be implemented.

The 3DoF model considers the aircraft to be a point-mass, where the center of mass is the rotational center where all forces apply. A further simplification of the 3DoF point-mass model in a vertical plane results in the so-called gamma-command model [31], in which vertical equilibrium is assumed. This is the model considered in this

[‡]Some aircraft models use slightly different names, such as certain Airbus models with the flight management and guidance system (FMGS) or even the flight management, guidance and envelope computer (FMGEC), in order to emphasize additional functionalities of those systems. In this article, however, we use the generic name of FMS to refer to the systems on-board providing flight trajectory planning and guidance.

contribution:

$$
\begin{aligned}
\frac{\mathrm{d}h}{\mathrm{d}t} &= \dot{h} = v \sin\gamma, \\
\frac{\mathrm{d}s}{\mathrm{d}t} &= \dot{s} = \sqrt{v^2 \cos^2\gamma - W_x^2} + W_s, \\
\frac{\mathrm{d}v}{\mathrm{d}t} &= \dot{v} = \frac{1}{m}\left[T(\pi, v, h) - D(v, h, m, \xi)\right] - g \sin\gamma, \\
\frac{\mathrm{d}m}{\mathrm{d}t} &= \dot{m} = -q(T, v, h),
\end{aligned}
\tag{1}
$$

where t is time, the state vector, $\mathbf{x} = [h,\ s,\ v,\ m]^T$, is composed of the geometric altitude, the along-path distance, the true airspeed, and the mass of the aircraft; and the generic control vector of this model, $\mathbf{u} = [\gamma,\ \pi]^T$, is given by the aerodynamic flight path angle γ (FPA) and the engine throttle π. T is the total thrust delivered by the aircraft engines, D is the aerodynamic drag, q is the total fuel flow, W_x is the cross-wind component, W_s is the along-path wind component, and g is the gravitational acceleration. It is worth noting that D also depends on the setting of the high-lift devices (i.e., flaps and/or slats) and landing gear, denoted above by ξ. The total engine thrust is modelled as $T = T_{\text{idle}} + \pi(T_{\text{max}} - T_{\text{idle}})$, where T_{idle} is the residual thrust delivered by the engines in idle setting ($\pi = 0$) and T_{max} is the thrust delivered for the maximum throttle setting ($\pi = 1$). An APM is required to model D, T_{idle}, T_{max} and q, as a function of some state variables. Similarly, a weather model is also required to model the wind components appearing in Eq. (1), but also to model certain aircraft performance variables that typically depend on air temperature and/or pressure.

Note that two degrees of freedom must be closed in order to integrate Equation (1) over time. Yet, they are seldom given in terms of engine throttle (π) and/or aerodynamic FPA (γ). Instead, the aircraft trajectory is typically divided into different phases or segments, and most of them are operated, for instance, at constant Mach or CAS. In some cases, climbs/descents could be specified at a constant vertical speed (i.e., rate of climb/descent) and acceleration/deceleration segments are computed keeping a constant energy share factor (ESF)[§]. These operational commands are referred to as *aircraft intent instructions*.

In [9], aircraft intent is defined as the *"the unambiguous description of the way that the aircraft is operated to effect the aircraft trajectory in accordance to the flight intent"*. The flight intent, in turn, encompasses the goals, constraints and preferences that are applicable to the flight, representing the objectives of the operator and needs to be achieved by the FMS. It could be seen as the *"the basic blueprint for trajectory computation"*, but it does not unambiguously determine the aircraft trajectory. Hence, the aircraft intent is the set of instructions that model operational commands or constraints on the aircraft behaviour, encompassing enough information to unequivocally describe and compute a 4D trajectory for a certain aircraft (given some initial conditions an atmospheric model and an APM). For more information,

[§]The constant energy share factor specifies the ratio of the rate of climb to the total energy (i.e., potential plus kinetic energy). See [36] and also Appendix A for its mathematical definition

the reader is referred to [9, 37], where a standardized method to describe trajectories was proposed by means of the Aircraft Intent Description Language (AIDL).

Taking this into consideration, the trajectory computation problem now becomes a sequence of Differential Algebraic Equation (DAE) problems, in order to model the different segments of the trajectory that are subject to different aircraft intent instructions. Since in this study we focus the vertical plane of the trajectory, two aircraft intent instructions are needed to steer the aircraft. Therefore, the DAE problem can be formulated as

$$\begin{aligned} \dot{\mathbf{x}} &= \mathbf{f}(\mathbf{x}, \mathbf{u}, \mathbf{p}, t) \\ c_1(\mathbf{x}, \mathbf{u}, \mathbf{p}, t) &= 0 \\ c_2(\mathbf{x}, \mathbf{u}, \mathbf{p}, t) &= 0 \end{aligned} \tag{2}$$

where the state ($\mathbf{x}$) and control ($\mathbf{u}$) vectors are also called, respectively, the vector of differential and algebraic variables. $\mathbf{p}$ is the vector of known guidance command parameters that are used to specify a particular intent instruction and $\mathbf{f}$ is the vector function that describes the state evolution, i.e., the motion of the aircraft as described in Eq. (1). Finally, c_1 and c_2 are the two algebraic constraints (also called path constraints in control theory) that mathematically model the two instructions of the aircraft intent needed to close the problem.

Equation (2) forms a system of DAEs that fully describes a trajectory in the vertical plane. Unless π and γ are directly given as a known input control sequence, it will be always needed to compute them first from the two instructions of the aircraft intent (i.e., solving c_1 and c_2 equations), in order to transform the original set of algebraic equations to a system of ODEs suitable for numerical integration.

The model presented above is an illustrative example of what one could find in a modern FMS. Yet, as commented before, the exact definition of the state and control vectors could vary, depending on the exact implementation. In fact, simpler models could be used for trajectory planning (at the expense of losing accuracy), or even table look-ups, which do not require numerical integration. The model presented above has been chosen to describe the dynamics of the aircraft in the filter presented in Sec. III and in the simulator of Sec. IV, used to validate the results. Appendix A contains the mathematical details for all pairs of algebraic constraints considered.

1. Example of an idle descent at constant speed

As long as the constraints on the arrival procedure allow, the FMS typically plans for an idle descent, starting with a constant Mach descent, followed by a constant CAS descent. The transition from Mach to calibrated airspeed descent phase is known as the cross-over altitude, where the true airspeed is the same for the given Mach and CAS. The values of Mach and CAS, respectively, are typically taken from pre-computed tables and aim to minimize a compound cost function of fuel and time, given the current flight conditions.

Hence, for this particular example, these two initial phases of the descent trajectory would be defined by

$$\begin{aligned} c_1 &\equiv \frac{\mathrm{d}(\cdot)}{\mathrm{d}t} = \frac{\partial(\cdot)}{\partial h}\dot{h} + \frac{\partial(\cdot)}{\partial v}\dot{v} = 0, \\ c_2 &\equiv \pi = 0, \end{aligned} \tag{3}$$

where $(\cdot)$ is either Mach (first phase) or CAS (second phase). The first algebraic equation imposes Mach and CAS to be constant (first intent instruction), whereas the second equation imposes idle thrust (second intent instruction).

Mach (M) and CAS (v_{CAS}) are modelled as a function of the state vector using information from the weather model. They are given by the following expressions:

$$M = \frac{v}{\sqrt{\gamma_a \tau R}}, \tag{4}$$

$$v_{\mathrm{CAS}} = \sqrt{\frac{2p_0}{\mu\rho_0}\left(\left(\frac{p}{p_0}\left(\left(\frac{\mu v^2}{2R\tau}+1\right)^{\frac{1}{\mu}}-1\right)+1\right)^{\mu}-1\right)}, \tag{5}$$

where γ_a is the specific heat ratio of the air; p and τ are pressure and temperature of the air; R is the perfect gas constant; $\mu = (\gamma_a - 1)\gamma_a^{-1}$; p_0 and ρ_0 are the standard pressure and density values at sea level.

The exact values for the Mach and CAS commands that will be chosen by the FMS ($\bar{M}$ and $\bar{v}_{\mathrm{CAS}}$) are represented by vector $\mathbf{p}$ in (2). As explained before, it will be needed to first solve the two algebraic equations (3) to obtain $\gamma(t)$ and $\pi(t)$ and, then, use these functions to integrate the ODE system depicted in (1).

2. Summary

A trajectory can be defined as a sequence of consecutive phases and, for each phase, two instructions that define the aircraft intent shall be given to specify the two path constraints that are needed to transform the DAE system into an ODE system to be numerically integrated. Note that for each phase at least one *exit condition* shall be defined as well, which will stop this integration and trigger the transition to the following phase. Moreover, certain models that are implicit in (1), such as aircraft drag, could change across different phases to consider, for instance, different flap/slat configurations, the deployment of the landing gear, the use of speedbrakes, etc.

B. Trajectory Guidance

The guidance part of the FMS embeds the logic that is executed to follow the previously planned trajectory. Typical aeroplanes have two independent actuators to steer their movement along the vertical plane: the elevator flight surface and the engine throttle. This means that among all the different (planned) variables that define a 4D trajectory, the guidance function of the FMS has to choose which two variables should be followed (or tracked) with these two actuators.

Assuming the FMS has perfect models when planning the trajectory, this would lead to the same 4D trajectory (and fuel consumption) as theoretically planned. But in a real flight, different sources of uncertainty are present, such as aircraft performance models, weather forecasts, actuator dynamics, etc. This means that the other variables that are not followed by the guidance system will differ from the plan. The guidance function of the FMS contains, in fact, a quite complex logic of different guidance modes and strategies that are switched from one to another during the flight execution, depending on many input variables, such as deviations with respect to the plan, the phase of the flight, operational conditions and flight envelope, capabilities of the actuators, etc.

Table 1 Climb/Descent Guidance Modes considered in this article

Command 1 (Elevator)	Command 2 (Throttle)	Parameters vector	Control vector
MACH		$\mathbf{p} = [\bar{M}, \bar{\pi}]$	$\pi(\mathbf{p}, \mathbf{x}) = \bar{\pi}$
CAS	THR	$\mathbf{p} = [\bar{v}_{\text{CAS}}, \bar{\pi}]$	
ACC/DEC		$\mathbf{p} = [\bar{k}_{esf}, \bar{\pi}]$	$\gamma(\mathbf{p}, \mathbf{x}) = \arcsin\left(\bar{k}_{esf}(T_{\text{idle}} + \bar{\pi}(T_{\max} - T_{\text{idle}}) - D)(mg)^{-1}\right)$ (†)
	MACH	$\mathbf{p} = [\bar{v}_h, \bar{M}]$	$\gamma(\mathbf{p}, \mathbf{x}) = \arcsin(\bar{v}_h / v)$
VS	CAS	$\mathbf{p} = [\bar{v}_h, \bar{v}_{\text{CAS}}]$	
	ACC/DEC	$\mathbf{p} = [\bar{v}_h, \bar{k}_{esf}]$	$\pi(\mathbf{p}, \mathbf{x}) = (D + \bar{k}_{esf}^{-1} mg \sin\gamma - T_{\text{idle}})(T_{\max} - T_{\text{idle}})^{-1}$ (†)
	MACH	$\mathbf{p} = [\bar{\gamma}_g, \bar{M}]$	$\gamma(\mathbf{p}, \mathbf{x}) = \arcsin\left(\sin\bar{\gamma}_g \left[\left(1 - \overline{W}_x^2 - \overline{W}_s^2 \sin^2\bar{\gamma}_g\right)^{1/2} + \overline{W}_s \cos\bar{\gamma}_g\right]\right)$ (‡†)
FPA	CAS	$\mathbf{p} = [\bar{\gamma}_g, \bar{v}_{\text{CAS}}]$	
	ACC/DEC	$\mathbf{p} = [\bar{\gamma}_g, \bar{k}_{esf}]$	$\pi(\mathbf{p}, \mathbf{x}) = (D + \bar{k}_{esf}^{-1} mg \sin\gamma - T_{\text{idle}})(T_{\max} - T_{\text{idle}})^{-1}$ (†)
VS		$\mathbf{p} = [\bar{v}_h, \bar{\pi}]$	$\pi(\mathbf{p}, \mathbf{x}) = \bar{\pi}$; $\gamma(\mathbf{p}, \mathbf{x}) = \arcsin(\bar{v}_h / v)$
FPA	THR	$\mathbf{p} = [\bar{\gamma}_g, \bar{\pi}]$	$\pi(\mathbf{p}, \mathbf{x}) = \bar{\pi}$; $\gamma(\mathbf{p}, \mathbf{x}) = \arcsin\left(\sin\bar{\gamma}_g \left[\left(1 - \overline{W}_x^2 - \overline{W}_s^2 \sin^2\bar{\gamma}_g\right)^{1/2} + \overline{W}_s \cos\bar{\gamma}_g\right]\right)$ (‡†)
ALT		$\mathbf{p} = [\bar{v}_h = 0, \bar{\pi}]$	$\pi(\mathbf{p}, \mathbf{x}) = \bar{\pi}$; $\gamma(\mathbf{p}, \mathbf{x}) = 0$
ALT	SPD	$\mathbf{p} = [\bar{v}_h = 0, \bar{M}]$	$\gamma(\mathbf{p}, \mathbf{x}) = 0$; $\pi(\mathbf{p}, \mathbf{x}) = (D - T_{\text{idle}})(T_{\max} - T_{\text{idle}})^{-1}$ (‡)

(†) The energy share factor k_{esf} is given as an input parameter for modes DEC or ACC ($\bar{k}_{esf}$); or computed as a function of $\bar{M}$ or $\bar{v}_{\text{CAS}}$ i MACH and CAS modes, respectively. See appendix A for details.

(‡) Note that the aerodynamic drag and maximum/idle thrust magnitudes depend on $\bar{M}$, along with other state variables

(‡†) $\overline{W}_s = W_s/v$ and $\overline{W}_x = W_x/v$ are the normalized components of the wind (head and cross wind, respectively).

1. Guidance modes

Next, the guidance commands considered in this article are listed, for the vertical plane and for a given configuration profile (i.e., high-lift devices, speedbrakes, and landing gear). The (known) input guidance command parameter associated to each command is also given:

- MACH: Constant Mach number ($\bar{M}$).

- `CAS`: Constant calibrated airspeed ($\bar{v}_{\mathrm{CAS}}$).
- `DEC`: Deceleration at a constant energy share factor ($\bar{k}_{esf}$).
- `ACC`: Acceleration at a constant energy share factor ($\bar{k}_{esf}$).
- `THR`: Fixed throttle setting ($\bar{\pi}$).
- `VS`: Constant vertical speed (rate of climb/descent) ($\bar{v}_h$).
- `FPA`: Constant ground FPA ($\bar{\gamma}_g$).
- `ALT`: Constant pressure altitude (zero vertical speed).
- `SPD`: Constant speed ($\bar{M}$ and $\bar{v}_{\mathrm{CAS}}$). Only used when the other guidance mode is `ALT`.

$\bar{M}, \bar{v}_{\mathrm{CAS}}, \bar{k}_{esf}, \bar{v}_h, \bar{\gamma}_g, \bar{\pi}$ are guidance command parameters constant values, i.e., vector $\mathbf{p}$ in (2); representing, respectively, Mach number, CAS, ESF, vertical speed, flight path angle relative to the ground, and throttle.

Table 1 lists all pairs of guidance commands considered in this article. The two commands in this table could be mapped with the longitudinal AIDL instructions that form the AIDL alphabet [9].

The 1st and 2nd columns identify the guidance commands that direct the two independent actuators of the aircraft (elevator and throttle). For each pair, the parameters $\mathbf{p}$ (i.e., known input guidance target) are given in the 3rd column. The command pairs of Table 1 are grouped by families:

- The first set of command pairs direct a fixed throttle setting ($\bar{\pi}$), while the elevator is used to command a certain speed or a certain acceleration/deceleration. These pairs of guidance commands are those typically found in climbs or descents. Aircraft typically climb at a fixed throttle setting, while keeping a constant CAS in the lower parts of the climb, or a constant Mach in the higher parts of the climb phase[¶]. Moreover, in a typical climb, different (short) acceleration phases are also found and these are typically performed at a constant ESF (accelerating and climbing at the same time). A descent is typically performed at a constant throttle setting, with constant Mach descents at higher altitudes, followed by constant CAS descents at lower ones. Deceleration descent phases are also performed at a given ESF.
- In the second set of command pairs, the elevator is commanded to keep a fixed vertical speed ($\bar{v}_h$), while the throttle is then commanded to maintain a certain speed or acceleration/deceleration. In a typical climb or descent, the (auto) pilot hardly ever steers the aircraft by keeping a constant rate of climb or descent. There are, however, some situations where these modes are used. For instance, in an early descent situation (when ATC clears the descent before reaching the top of decent planned by the FMS), the guidance system will typically command `VS-MACH` (which can be followed by a `VS-CAS` at lower altitudes) in order to intercept the planned descent from below [38]. This type of guidance might also be found in the so-called "re-pressurization segments", sometimes found at the beginning of the descent phase in which the vertical speed is limited to permit a proper cabin

[¶]In the lower atmosphere, the maximum CAS in operations (named VMO) is more limiting than the maximum Mach in operations (MMO) and CAS is the operational speed used. At higher altitudes, however, MMO becomes more limiting than VMO and Mach number becomes the operational speed.

re-pressurization. Furthermore, in certain situations, ATC might request the aircraft crew to climb/descent at a rate of climb/descent.

- The third set commands the elevator to keep a fixed ground FPA ($\bar{\gamma}_g$), while the throttle is commanded to maintain a certain speed or acceleration/deceleration. Like the previous guidance family, these pairs are activated in very specific situations, especially in the descent phase. When an idle descent cannot be planned because of altitude and/or speed restrictions in the destination terminal airspace, the FMS typically plans segments of constant ground FPA that geometrically join certain navigation waypoints overflying them at specific altitudes. Then, `FPA-MACH` or `FPA-CAS` will be commanded. Another typical example is when the aircraft is established in the instrumental landing system glide slope, in the final approach segment. The aircraft would command either `FPA-DEC` if decelerating or `FPA-CAS` if keeping a constant airspeed (in the last part of the final approach, with the aircraft fully configured and stabilized for landing).
- In the fourth set, the elevator is dedicated to follow a specific vertical trajectory profile (either at constant vertical speed, constant ground FPA, or a constant pressure altitude), while a fixed throttle setting is given ($\bar{\pi}$). These pairs are rarely used, except for `ALT-THR`, which is found in level-offs to (quickly) accelerate or decelerate the aircraft (depending on the thrust setting).
- The last command pair in Table 1 corresponds to the particular case where constant altitude and speed shall be followed. Since the pressure altitude is constant, keeping a constant Mach is equivalent to follow a constant CAS, and vice-versa. This corresponds to cruise flight, but also to level-offs at constant speed, typically found in terminal airspace when sequencing and merging traffic and/or for certain segments in the depart or approach procedures.

2. Computing the control vector

As explained in Sec. II.A, throttle and FPA in (1) are seldom chosen as the instructions for the aircraft intent to plan a trajectory. Similarly, they are not typically used as guidance commands to steer the aircraft in the execution phase of the flight. Thus, in order to properly model all different system models, it is required to express the control vector as a function of the (known) guidance parameters for each pair. This computation is also needed by the in-house trajectory simulator to generate validation trajectories.

The mathematical relationship between intents (or guidance modes) and controls is given in the last column of Table 1, while the Appendix gives the mathematical details. Although the case studies presented in this article assume no winds and international standard atmosphere (ISA) conditions, Table 1 provides the general control vector expressions.

III. Methodology

The goal of this contribution is to propose a method able to identify in real-time the active guidance modes (GMs) that is steering the trajectory of a particular aircraft (i.e., a GM contains a command pair), by observing only surveillance data. Because the lateral path uncertainty is much lower than the vertical one [10], the focus is on the vertical profile.

Three equations are needed to formulate the problem: 1) $\mathbf{f}(\mathbf{x}, \mathbf{u})$ describes the state evolution; 2) $\mathbf{y} = \mathbf{h}(\mathbf{x})$ describes the link between measurements and the states to be inferred; and 3) each guidance command pair is associated to a pair of algebraic expressions (c_1 and c_2) that relate the guidance commands of each mode and the control vector $\mathbf{u}(\mathbf{p}, \mathbf{x})$. Solving (2) for the different pairs depicted in Table 1 leads to $N = 25$ ($2 \times 12 + 1$) possible aircraft GMs for a typical climb/descent (i.e., all the modes except for `ALT-SPD` may have clean or non-clean configurations). That is, the problem formulation is given by a set of N nonlinear discrete state-space models (SSMs). This can be written as a jump Markov system,

$$\mathbf{x}_k = \mathbf{f}_{k-1}(\mathbf{x}_{k-1}, \mathbf{u}_{k-1}(\mathbf{p}(\theta_k), \mathbf{x}_{k-1}), \theta_k) + \mathbf{w}_{k-1}, \tag{6a}$$

$$\mathbf{y}_k = \mathbf{h}_k(\mathbf{x}_k) + \mathbf{v}_k, \tag{6b}$$

where $\theta_k \in \{1, 2, \ldots, N\}$ is the mode state, that is, each value of the discrete random variable θ_k leads to a different SSM. Here k refers to the discrete-time instants; $\mathbf{x}_k$ and $\mathbf{y}_k$ are the state and observation vector at time k; $\mathbf{f}_{k-1}(\cdot)$ and $\mathbf{h}_k(\cdot)$ are known nonlinear system model functions; $\mathbf{w}_{k-1}$ and $\mathbf{v}_k$ are the process and measurement noise.

A. Measurements

The measurements available come from ADS-B and EHS data broadcast by the aircraft:

- ADS-B is a data-link-based surveillance technology that can be exploited for both air-ground and air-air applications. This allows aircraft to send the identification, position, ground speed, and other flight parameters (such as rate of climb/descent, which is the time derivative of the pressure altitude; or inertial vertical speed, which is the time derivative of the geometric altitude), coming from on-board air data and navigation systems [39].
- EHS technology is a secondary surveillance radar-dependent protocol with additional flight parameters (e.g., the true airspeed, indicated airspeed, ground speed, Mach number, and true heading of the aircraft). Indeed, several Comm-B Data Selector (BDS) messages are identified as EHS: i) vertical intention report from BDS 40 (select altitude, barometric pressure setting); ii) track and turn report from BDS 50 (roll angle, track angle, ground speed, track angle rate, true airspeed); and iii) heading and speed report from BDS 60 (magnetic heading, indicated airspeed, Mach number, vertical velocity) [39].

The measurements available from ADS-B and EHS considered in this article are $\mathbf{y} = [h_p, v_g, v_h, v_{CAS}, M]^\top$; with h_p the pressure altitude, v_g the ground speed, v_h the aircraft (operational) vertical speed (i.e., the pressure altitude

change rate), v_{CAS} the calibrated airspeed (taken from the indicated airspeed broadcast by ADS-B) and M the Mach number.

B. Further Details on the System Model

With respect to (1), two additional variables are considered: τ is the temperature and p is the air pressure. The complete state to be inferred is $\mathbf{x} = [h, s, v, m, \tau, p]^\top$, with

$$\frac{\mathrm{d}\tau}{\mathrm{d}t} = \dot{\tau} = \tau_h(h)\dot{h}, \ \frac{\mathrm{d}p}{\mathrm{d}t} = \dot{p} = p_h(\tau, p)\dot{h}, \tag{7}$$

where τ_h and p_h are, respectively, the partial derivative of the temperature and pressure with respect to the altitude. The complete process function is then obtained from (1), expressing the dynamics of the aircraft, and (7). Notice that the control vector $\mathbf{u} = [\gamma, \pi]^\top$ is rewritten as $\mathbf{u}_{k-1}(\mathbf{p}(\theta_k), \mathbf{x}_{k-1})$, where at each time instant k, for the corresponding mode θ_k, the values of γ and π are detailed in Table 1.

In this contribution, we consider that both process and measurement noise are Gaussian distributed, being a valid assumption under optimal conditions (i.e., no impulsive or heavy-tailed behaviours in the aircraft dynamics that can be assumed to be smooth, and electronic thermal noise in the measurement devices), $\mathbf{w}_k \sim \mathcal{N}(\mathbf{0}, \mathbf{Q}_k)$ and $\mathbf{v}_k \sim \mathcal{N}(\mathbf{0}, \mathbf{R}_k)$.

C. Filtering Strategy

The nonlinear Bayesian filtering for the system in (6a)-(6b) does not admit a closed-form solution and suboptimal techniques must account for the nonlinear system of interest. The best performance is typically obtained by resorting to the IMM particle filter [40], but the price is high computational complexity. If noise distributions are Gaussian, one can resort to sigma-point filter-based IMM approaches [41, 42], which use a bank of sigma-point filters, each one matched to a given SSM. For the problem at hand, because we seek the optimal performance under optimal conditions (i.e., small noise assumption), the sigma-point filter and extended Kalman filter (EKF) performance is equivalent. Therefore, in this contribution, and without loss of generality, we consider an EKF-IMM (i.e., IMM filter with a bank of N EKFs). Fig. 1 depicts the specific workflow of the EKF-IMM algorithm: i) interaction (or reinitialisation); ii) model-based filtering; and iii) combination (estimate fusion).

D. EKF-IMM Algorithm

The IMM-based filtering approach uses a bank of N filters each one matched to a single SSM, then computes the posterior mode probabilities $\{\mu_k^i = P(\theta_k = i|\mathbf{y}_{1:k})\}_{i=1}^N$, with $\mathbf{y}_{1:k}^\top = [\mathbf{y}_1^\top, \ldots, \mathbf{y}_k^\top]$, and constructs the final estimate/covariance as a combination of individual EKF estimates $\widehat{\mathbf{x}}_{k|k}^i$, with associated covariance $\mathbf{P}_{k|k}^i$. Then, the question is how to recursively compute the mode conditional $\widehat{\mathbf{x}}_{k|k}^i$, $\mathbf{P}_{k|k}^i$, and μ_k^i.

- *Interaction step*: If one considers a transition probability matrix Π where its elements $r_{ji} = P(\theta_k = i|\theta_{k-1} = j)$

define the probability to jump from mode j to mode i, the i-th *mixed* filter input is

$$\widehat{\mathbf{x}}^{0i}_{k-1|k-1} = \sum_{j=1}^{N} \mu^{ji}_{k-1|k-1} \widehat{\mathbf{x}}^{j}_{k-1|k-1}, \tag{8a}$$

$$\mathbf{P}^{0i}_{k-1|k-1} = \sum_{j=1}^{N} \mu^{ji}_{k-1|k-1} \left[\mathbf{P}^{j}_{k-1|k-1} + \left(\widehat{\mathbf{x}}^{j}_{k-1|k-1} - \widehat{\mathbf{x}}^{0i}_{k-1|k-1} \right) (\cdot)^{\top} \right],$$

with mixing probabilities

$$\mu^{ji}_{k-1|k-1} = \frac{r_{ji} \mu^{i}_{k-1}}{\sum_{l=1}^{N} \pi_{li} \mu^{l}_{k-1}}. \tag{9}$$

- *Filtering step*: In this step, each EKF is matched to a GM. The i-th EKF prediction and update equations are

$$\begin{aligned}
\widehat{\mathbf{x}}^{i}_{k|k-1} &= \mathbf{f}_{k-1}(\widehat{\mathbf{x}}^{0i}_{k-1|k-1}, \mathbf{u}_{k-1}(\mathbf{p}(i), \widehat{\mathbf{x}}^{0i}_{k-1|k-1}), i), \\
\mathbf{P}^{i}_{k|k-1} &= \mathbf{F}^{i}_{k-1} \mathbf{P}^{0i}_{k-1|k-1} (\mathbf{F}^{i}_{k-1})^{\top} + \mathbf{Q}_{k-1}, \\
\mathbf{S}^{i}_{k|k-1} &= \mathbf{H}^{i}_{k} \mathbf{P}^{i}_{k|k-1} (\mathbf{H}^{i}_{k})^{\top} + \mathbf{R}_{k}, \\
\mathbf{K}^{i}_{k} &= \mathbf{P}^{i}_{k|k-1} (\mathbf{H}^{i}_{k})^{\top} (\mathbf{S}^{i}_{k|k-1})^{-1}, \\
\widehat{\mathbf{x}}^{i}_{k|k} &= \widehat{\mathbf{x}}^{i}_{k|k-1} + \mathbf{K}^{i}_{k} (\mathbf{y}_{k} - \mathbf{h}_{k}(\widehat{\mathbf{x}}^{i}_{k|k-1})), \\
\mathbf{P}^{i}_{k|k} &= \left(\mathbf{I} - \mathbf{K}^{i}_{k} \mathbf{H}^{i}_{k} \right) \mathbf{P}^{i}_{k|k-1},
\end{aligned}$$

  where $\mathbf{F}^{i}_{k-1}$ is the Jacobian of $\mathbf{f}_{k-1}(\cdot, \cdot, i)$ evaluated at $\widehat{\mathbf{x}}^{0i}_{k-1|k-1}$, and $\mathbf{H}^{i}_{k}$ is the Jacobian of $\mathbf{h}_{k}(\cdot)$ evaluated at $\widehat{\mathbf{x}}^{i}_{k|k-1}$. Notice that $\mathbf{y}_{k} - \mathbf{h}_{k}(\widehat{\mathbf{x}}^{i}_{k|k-1})$ is the so-called innovation vector, with associated covariance $\mathbf{S}^{i}_{k|k-1}$. This innovation carries information about the fit between the observed data and the model used to compute the estimate (i.e., model likelihood).

- *Mode probability update*: To update the mode probability μ^{i}_{k} from μ^{i}_{k-1} for a Gaussian system, are

$$\mu^{i}_{k} = \frac{\mathcal{N}(\widehat{\mathbf{y}}^{i}_{k|k-1}, \mathbf{S}^{i}_{k|k-1}) \sum_{j=1}^{N} \pi_{ji} \mu^{j}_{k-1}}{\sum_{l=1}^{N} \mathcal{N}(\widehat{\mathbf{y}}^{l}_{k|k-1}, \mathbf{S}^{l}_{k|k-1}) \sum_{j=1}^{N} \pi_{jl} \mu^{l}_{k-1}}. \tag{10}$$

- *Fusion step*: The final estimate/covariance as

$$\widehat{\mathbf{x}}_{k|k} = \sum_{i=1}^{N} \mu^{i}_{k} \widehat{\mathbf{x}}^{i}_{k|k}, \tag{11a}$$

$$\mathbf{P}_{k|k} = \sum_{i=1}^{N} \mu^{i}_{k} \left[\mathbf{P}^{i}_{k|k} + \left(\widehat{\mathbf{x}}^{i}_{k|k} - \widehat{\mathbf{x}}_{k|k} \right) (\cdot)^{T} \right], \tag{11b}$$

  where $\widehat{\mathbf{x}}^{i}_{k|k}$ is the i-th EKF estimate, and $\mathbf{P}^{i}_{k|k}$ the corresponding estimation error covariance.

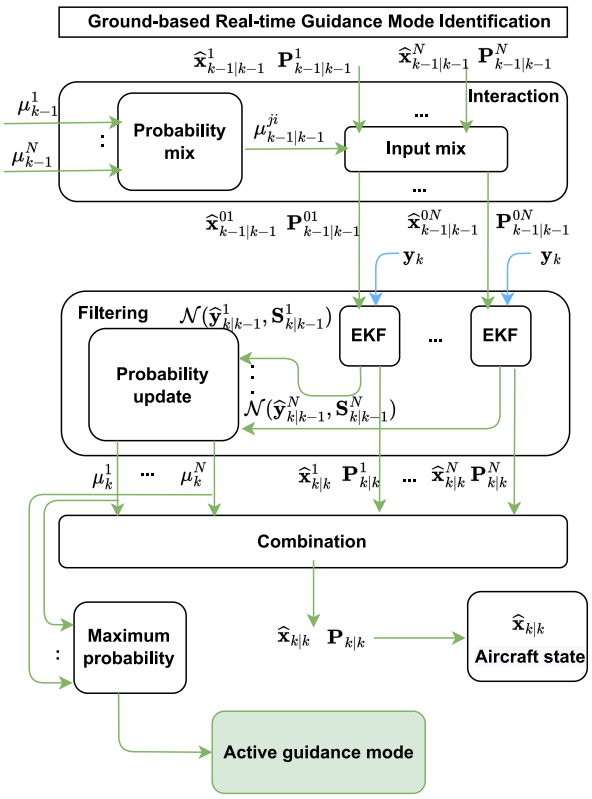

Fig. 1 The EKF-IMM flow diagram.

E. Guidance Mode Identification

Notice that the output of the EKF-IMM provides at each time step k the state vector estimate $\widehat{\mathbf{x}}_{k|k}$, its associated covariance $\mathbf{P}_{k|k}$, and also the model probability for each guidance mode μ_k^i. Even if it is not the standard use of IMM-based filters, μ_k^i can be exploited for model identification. Indeed, the identified GM is taken as the one with largest mode probability (i.e., the most likely one),

$$\widehat{\mathrm{GM}}_k = \arg\max_i \left\{ [\mu_k^1, \ldots, \mu_k^N] \right\}. \tag{12}$$

Notice that the maximum mode probability will be larger if the different modes in the pool of candidates are very distinct, and lower if the modes are close to each other (i.e., competing modes). This implies that to obtain a good mode identification the user must avoid close or unidentifiable modes. Illustrative examples of this issue are shown in Sec. V.

IV. Results with Simulated Trajectories

A custom trajectory simulator is used to generate 3D climb/descent trajectories (2D in the vertical plane plus time), which builds upon a gamma-command aircraft motion model [31], and the BADA v4.1 APM [43]. The APM is used to define, for instance, the aircraft forces (e.g., thrust and drag) and fuel flow. A performance model of a representative

narrow-body airliner has been chosen. The custom trajectory simulator emulates data based on real trajectories. Indeed, emulated profiles are inspired by comprehensive experimental analysis on real data and flight experiments.

A. Guidance Modes and Validation Trajectories

Recall that a trajectory is unequivocally specified by a sequence of phases, described by two guidance commands and an end condition. Such definition provides the three key ingredients to simulate a realistic trajectory:

- *Trajectory phases*: The vertical profile of the trajectory is split into a finite number of phases. Each phase is specified by two guidance commands and an end condition. Different phases can also be used to model different flaps and/or landing gear configurations or engine thrust ratings.
- *Guidance commands and parameters*: Guidance commands steer the aircraft through elevator and throttle. At each phase the parameters are used to compute the control vector, $\mathbf{u} = [\gamma, \pi]$ (refer to Table 1).
- *End condition*: This term specifies the conditions to model the transition between phases, where guidance commands and/or aerodynamic conditions (flaps/slats, landing gear position, etc) change[‖].

A set of six representative validation trajectories (VTs) are considered: four descents and two climbs. A brief description of these VTs is given in Tables 2–7. The initial conditions (IC) of the numerical integration are taken above the runway, leading to a forward integration for climbs and a backward integration for descents. Thus, the sequence of phases in these tables is always given from the runway to cruise. Notice the IC for VT5 and VT6, where $h_p = 50\,\text{ft}$ including, thus, the final descent/initial climb. FL stands for flight level. In the vertical profiles, Δs refers to the distance-to-go (along-path distance) of an aircraft during a given phase.

In the first four VTs, `CLEAN-UP` refers to the case where flaps/slats and landing gear are not deployed. For the last two VTs, which include lower altitudes down to the runaway, the flaps/slats (i.e., the most relevant positions in Airbus are modeled as `FULL`, `CONF 3, 2, 1`, or `CLEAN` to guide the aircraft) and landing gear (i.e., `DOWN` or `UP`) are progressively retracted in the take-off and initial climb, and progressively deployed in the final approach and landing phase.

Fig. 2 illustrates the simulated flight data, including altitude, true airspeed, calibrated airspeed, and Mach number versus distance-to-go. The vertical purple lines indicate the end of each phase. Because a backward integration is used for descent profiles, the distance-to-go values are negative.

To further complement the information provided in Tables 2–7 and Figure 2, more details are given in the sequel:

- VT1: This VT illustrates a typical early descent trajectory, where the aircraft starts to descend before reaching the planned top of descent. In this situation, the FMS typically commands a descent at constant vertical speed to intercept the planned path from below. In our VT, this segment is modelled at constant calibrated airspeed, and it is followed by a sequence of phases where the aircraft flies at idle thrust and decelerates to reach 3000 ft at 230 kt

[‖] As an example, consider a phase where the two commands are constant Mach and idle thrust (`MACH-THR`), until the moment that calibrated airspeed achieves a given value (i.e., reaching that specific CAS is the phase end condition); then, the aircraft is flown at constant calibrated airspeed and constant vertical speed, being the new phase commands (`VS-CAS`).

Table 2 Vertical descent profile specification of VT1

IC: $h_p = 3000\,\text{ft}$, $s = 0\,\text{NM}$, $v_{\text{CAS}} = 230\,\text{kt}$, $m = 60000\,\text{kg}$

Phase	GM	Command1	Command2	End Condition	Configuration
1	CAS-THR	$\bar{v}_{\text{CAS}} = 230\,\text{kt}$	$\bar{\pi} = 0$	$h_p = \text{FL100}$	CLEAN-UP
2	DEC-THR	$\bar{k}_{esf} = 0.3$	$\bar{\pi} = 0$	$v_{\text{CAS}} = 280\,\text{kt}$	CLEAN-UP
3	CAS-THR	$\bar{v}_{\text{CAS}} = 280\,\text{kt}$	$\bar{\pi} = 0$	$h_p = \text{FL280}$	CLEAN-UP
4	VS-CAS	$\bar{v}_h = -1000\,\text{ft/min}$	$\bar{v}_{\text{CAS}} = 280\,\text{kt}$	$M = 0.8$	CLEAN-UP
5	ALT-MACH	$\bar{v}_h = 0$ ($h_p = \text{FL360}$)	$\bar{M} = 0.8$	$\Delta s = 20\,\text{NM}$	CLEAN-UP

Table 3 Vertical descent profile specification of VT2

IC: $h_p = 3000\,\text{ft}$, $s = 0\,\text{NM}$, $v_{\text{CAS}} = 250\,\text{kt}$, $m = 58000\,\text{kg}$

Phase	GM	Command1	Command2	End Condition	Configuration
1	FPA-CAS	$\bar{\gamma}_g = -3\,\text{deg}$	$\bar{v}_{\text{CAS}} = 250\,\text{kt}$	$h_p = \text{FL100}$	CLEAN-UP
2	DEC-THR	$\bar{k}_{esf} = 0.3$	$\bar{\pi} = 0$	$v_{\text{CAS}} = 300\,\text{kt}$	CLEAN-UP
3	CAS-THR	$\bar{v}_{\text{CAS}} = 300\,\text{kt}$	$\bar{\pi} = 0$	$h_p = \text{FL300}$	CLEAN-UP
4	MACH-THR	$\bar{M} = 0.8$	$\bar{\pi} = 0$	$h_p = \text{FL360}$	CLEAN-UP
5	ALT-MACH	$\bar{v}_h = 0$ ($h_p = \text{FL360}$)	$\bar{M} = 0.8$	$\Delta s = 20\,\text{NM}$	CLEAN-UP

Table 4 Vertical descent profile specification of VT3

IC: $h_p = 3000\,\text{ft}$, $s = 0\,\text{NM}$, $v_{\text{CAS}} = 192\,\text{kt}$, $m = 53000\,\text{kg}$

Phase	GM	Command1	Command2	End Condition	Configuration
1	DEC-THR	$\bar{k}_{esf} = 0.3$	$\bar{\pi} = 0$	$v_{\text{CAS}} = 250\,\text{kt}$	CLEAN-UP
2	CAS-THR	$\bar{v}_{\text{CAS}} = 250\,\text{kt}$	$\bar{\pi} = 0$	$h_p = \text{FL100}$	CLEAN-UP
3	DEC-THR	$\bar{k}_{esf} = 0.3$	$\bar{\pi} = 0$	$v_{\text{CAS}} = 330\,\text{kt}$	CLEAN-UP
4	CAS-THR	$\bar{v}_{\text{CAS}} = 330\,\text{kt}$	$\bar{\pi} = 0$	$M = 0.77$	CLEAN-UP
5	MACH-THR	$\bar{M} = 0.77$	$\bar{\pi} = 0$	$h_p = \text{FL350}$	CLEAN-UP
6	ALT-MACH	$\bar{v}_h = 0$ ($h_p = \text{FL350}$)	$\bar{M} = 0.77$	$\Delta s = 50\,\text{NM}$	CLEAN-UP

Table 5 Vertical climb profile specification of VT4

IC: $h_p = 2300\,\text{ft}$, $s = 0\,\text{NM}$, $v_{\text{CAS}} = 250\,\text{kt}$, $m = 77000\,\text{kg}$

Phase	GM	Command1	Command2	End Condition	Configuration
1	CAS-THR	$\bar{v}_{\text{CAS}} = 250\,\text{kt}$	$\bar{\pi} = 1$	$h_p = \text{FL100}$	CLEAN-UP
2	ACC-THR	$\bar{k}_{esf} = 0.3$	$\bar{\pi} = 1$	$v_{\text{CAS}} = 290\,\text{kt}$	CLEAN-UP
3	CAS-THR	$\bar{v}_{\text{CAS}} = 290\,\text{kt}$	$\bar{\pi} = 1$	$M = 0.77$	CLEAN-UP
4	MACH-THR	$\bar{M} = 0.77$	$\bar{\pi} = 1$	$h_p = \text{FL340}$	CLEAN-UP
5	ALT-MACH	$\bar{v}_h = 0$ ($h_p = \text{FL340}$)	$\bar{M} = 0.77$	$\Delta s = 50\,\text{NM}$	CLEAN-UP

Table 6 Vertical descent profile specification of VT5

IC: $h_p = 50\,\text{ft}$, $s = 0\,\text{NM}$, $v_{\text{CAS}} = 128\,\text{kt}$, $m = 53000\,\text{kg}$

Phase	GM	Command1	Command2	End Condition	Configuration
1	FPA-CAS	$\bar{\gamma}_g = -3\,\text{deg}$	$\bar{v}_{\text{CAS}} = 128\,\text{kt}$	$h_p = 1000\,\text{ft}$	FULL-DOWN
2	FPA-DEC	$\bar{\gamma}_g = -3\,\text{deg}$	$\bar{k}_{esf} = 0.472$	$v_{\text{CAS}} = 146.5\,\text{kt}$	FULL-DOWN
3	FPA-DEC	$\bar{\gamma}_g = -3\,\text{deg}$	$\bar{k}_{esf} = 0.53$	$v_{\text{CAS}} = 165\,\text{kt}$	CONF3-DOWN
4	FPA-DEC	$\bar{\gamma}_g = -3\,\text{deg}$	$\bar{k}_{esf} = 0.683$	$h_p = 2000\,\text{ft}$	CONF2-UP
5	FPA-DEC	$\bar{\gamma}_g = -3\,\text{deg}$	$\bar{k}_{esf} = 0.76$	$h_p = 3000\,\text{ft}$	CONF1-UP
6	VS-CAS	$\bar{v}_h = -1000\,\text{ft/min}$	$\bar{v}_{\text{CAS}} = 193\,\text{kt}$	$\Delta s = 50\,\text{NM}$	CONF1-UP
7	DEC-THR	$\bar{k}_{esf} = 0.3$	$\bar{\pi} = 0$	$v_{\text{CAS}} = 250\,\text{kt}$	CLEAN-UP
8	CAS-THR	$\bar{v}_{\text{CAS}} = 250\,\text{kt}$	$\bar{\pi} = 0$	$h_p = \text{FL100}$	CLEAN-UP

Table 7 Vertical climb profile specification of VT6

IC: $h_p = 50\,\text{ft}$, $s = 0\,\text{NM}$, $v_{\text{CAS}} = 158\,\text{kt}$, $m = 77000\,\text{kg}$

Phase	GM	Command1	Command2	End Condition	Configuration
1	CAS-THR	$\bar{v}_{\text{CAS}} = 158\,\text{kt}$	$\bar{\pi} = 1$	$h_p = 1500\,\text{ft}$	CONF2-UP
2	ACC-THR	$\bar{k}_{esf} = 0.3$	$\bar{\pi} = 1$	$v_{\text{CAS}} = 172\,\text{kt}$	CONF2-UP
3	ACC-THR	$\bar{k}_{esf} = 0.3$	$\bar{\pi} = 1$	$v_{\text{CAS}} = 212\,\text{kt}$	CONF1-UP
4	ACC-THR	$\bar{k}_{esf} = 0.3$	$\bar{\pi} = 1$	$v_{\text{CAS}} = 250\,\text{kt}$	CLEAN-UP
5	CAS-THR	$\bar{v}_{\text{CAS}} = 250\,\text{kt}$	$\bar{\pi} = 1$	$h_p = \text{FL100}$	CLEAN-UP

in clean configuration and landing gear up.

- VT2 & VT3: These trajectories illustrate two typical descents down to 3000 ft. Both trajectories follow a typical MACH-THR, CAS-THR descent at idle thrust down to FL100. Besides the Mach-CAS values chosen for this initial descent, the main difference between both VTs is on the final part of the trajectory, from FL100 down to 3000 ft. While in VT2, the elevator command is on the FPA and the throttle is settled to keep the constant calibrated airspeed, VT3 divides this last part into two phases, where the throttle is fixed to idle and the elevator either controls the calibrated airspeed, or reduces the speed, respectively. Both VTs are flown in clean configuration and landing gear up.
- VT4: The fourth VT illustrates a typical CAS-THR, MACH-THR climb trajectory starting at 250 kt and 2300 ft above the runway, until the cruise altitude is reached, considering a clean flaps/slats configuration and landing gear up. In this climb profile, the throttle is always set at the highest rate, assuming maximum climb thrust. The other actuator (i.e., the elevator) is dedicated to control the aircraft acceleration/speed.
- VT5 & VT6: These VTs illustrate representative descent and climb trajectories at lower altitudes (between FL100 and 50ft above the runway). For these trajectories, high-lift devices and landing gear deployment are modelled.

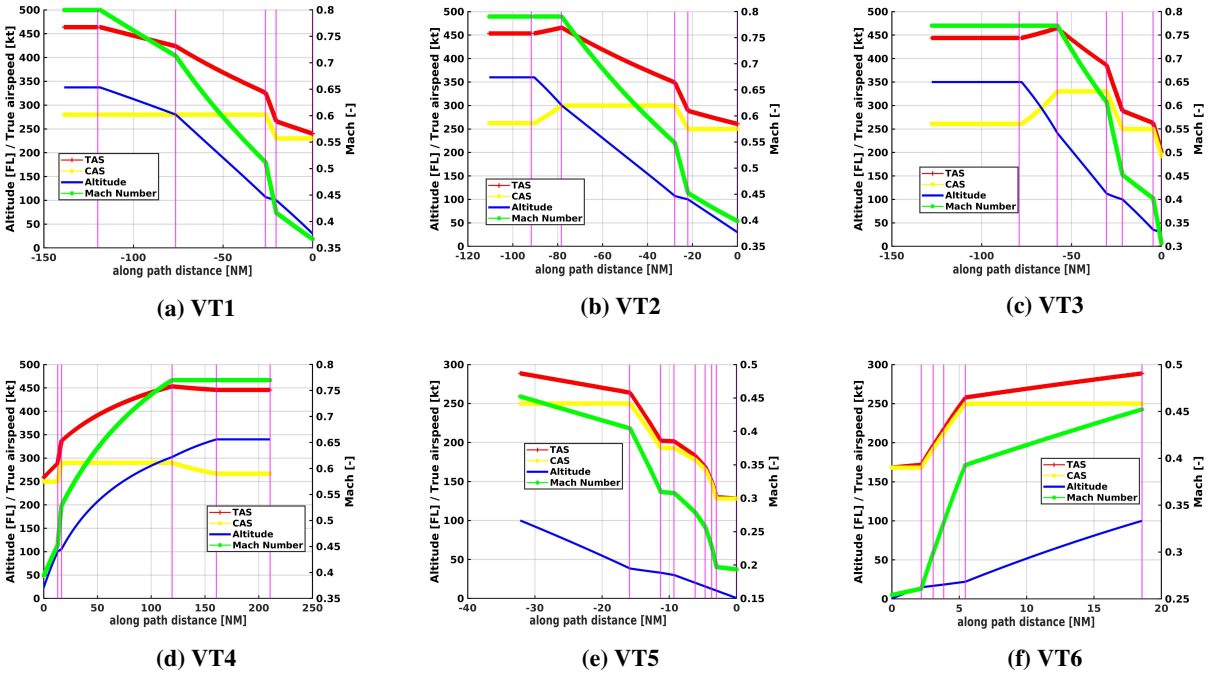

(a) VT1 **(b) VT2** **(c) VT3**

(d) VT4 **(e) VT5** **(f) VT6**

Fig. 2 Validation trajectories.

- VT5: The descent starts with idle thrust and constant speed/deceleration (phases 8 and 7). The first flaps/slats position is deployed while the elevator controls the constant vertical speed and the speed is managed by the throttle (`VS-CAS`). In the subsequent phases, flaps/slats positions are progressively deployed, with the elevator commanding a constant ground FPA (assuming an instrumental landing system glide path is flown), while the throttle commands different deceleration rates until phase 1, where a constant calibrated airspeed is kept. Landing gear is deployed in phases 1-2-3.
- VT6 The throttle is always set at the maximum rate and the acceleration/speed is controlled by the elevator. Flaps/slats positions are progressively retracted during this climb and gear is always up.

B. Further Assumptions

According to Table 1, N=25 guidance pairs could be considered. Among these modes, 13 are related to modes with retracted configurations, and 12 consider different positions of flap/slats and landing gear—named as `non-clean`—to emulate realistic flight phases. Among all pairs, `ALT-SPD` is the only one with always `clean` configuration. The drag coefficient (considered known) must be computed to obtain the aerodynamic drag force. From [43], such a drag coefficient is defined considering `clean` or `non-clean` configurations. The goal is to assess the EKF-IMM capabilities to distinguish between both configurations. It is worth mentioning that the throttle is either set to 1 for climbs (maximum rate) or 0 for descents (minimum rate) when `THR` is an active mode ($\bar{\pi} \in \{0, 1\}$). $\mathbf{p}$ is also assumed to be known.

The case studies presented in this section assume no winds and ISA conditions. Then, for altitudes below the

tropopause altitude, $\tau_h = -\lambda_\tau$ in (7) (λ_τ the temperature lapse rate). In hydrostatic equilibrium and regardless of the pressure altitude, $p_h = -\rho g$, where the density of the air is $\rho = p/R\tau$. Noting that $\dot{h}$ and v_h depend on temperature and its deviation $\Delta\tau$, the latter in ISA conditions is $0K$, then $h_p = h$ and $v_h = \dot{h}$.

Within the EKF-IMM, a time-invariant transition probability matrix is considered, with $r_{ji} = 0.02$ for $j \neq i$ and $r_{ii} = 0.98$. The initial system state $\mathbf{x}_0$ can be obtained from measurements except for the aircraft mass. The initial aircraft mass is considered to be shared by the airline (airlines can deliver it depending on their policy and data confidentiality).

C. Monte Carlo Analysis Results

Results for both GM identification and state estimation are provided hereafter. To obtain statistically meaningful results, 500 Monte Carlo (MC) runs are performed. The simulation set up is as follows: i) generate the noiseless simulated data to emulate a flight for an airbus A320 in the vertical plane; ii) add random Gaussian measurement and process noise for each MC run ($\mathbf{R}$ a diagonal matrix with $\mathbf{R}_{11} = 30^2[ft]$, $\mathbf{R}_{22} = 2.4^2[kt]$, $\mathbf{R}_{33} = 25^2[ft/min]$, $\mathbf{R}_{44} = 2.3^2[kt]$ and $\mathbf{R}_{55} = 0.003$; and $\mathbf{Q}$ a diagonal matrix with $\mathbf{Q}_{ii} = 0.001^2$ for $i = 1$ to 6); iii) estimate the aircraft trajectory and identify the guidance modes for each MC run; and iv) obtain the final average results. While steps ii) and iii) are performed at each Monte Carlo run (with a different noise realisation), step (i) is performed only once for each validation trajectory, and step (v) is performed only once after the 500 MC runs. The average root mean square error (RMSE) over the trajectory is taken as the measure of state estimation performance. For GM identification, the measure of performance is the percentage of the trajectory time where the algorithm provides an erroneous identification, denoted e_{ident}. The IMM-based GM identification results are summarized in Table 8.

Table 8 Average RMSE and guidance mode identification IMM-based results for the six representative VTs.

	VT1	VT2	VT3	VT4	VT5	VT6
e_{ident}	2.81 %	3.00 %	0.08 %	0.05 %	7.26 %	0.35 %
mean-RMSE						
h	10.47 ft	11.16 ft	13.00 ft	2.78 ft	6.91 ft	1.96 ft
s	0.06 NM	0.07 NM	0.07 NM	0.02 NM	0.01 NM	0.001 NM
v	0.56 kt	0.58 kt	0.51 kt	0.49 kt	0.53 kt	0.08 kt
m	70.41 kg	51.19 kg	7.68 kg	0.87 kg	5.51 kg	0.26 kg
τ	0.24 K	0.24 K	0.28 K	0.21 K	0.39 K	0.14 K
p	33.42 Pa	42.03 Pa	49.28 Pa	23.33 Pa	34.25 Pa	13.84 Pa

First, we can clearly see the good behaviour of the proposed solution (on average) for the trajectories that do not take into account some flap/slats (and landing gear) configurations, where e_{ident} is below 0.1% for the descent VT3 and climb VT4, and below 3% for descents VT1 and VT2. For VT6, which represents an initial climb, the IMM is

also performing very well, with $e_{ident} = 0.35\%$. The most challenging VT is VT5, which contains different positions of flap/slats and landing gear and illustrates a realistic final descent, for which $e_{ident} = 7.26\%$. Even if this value is significantly larger than the ones obtained for the other VTs, notice that most of the time the method correctly identifies the active GM. The latter will be further discussed when considering the estimated guidance mode versus along-path distance.

The mean RMSE results in Table 8 also support the good performance statement. Notice for instance that the mean RMSE for the altitude is always below 13 ft, and 0.07 NM for the along-path distance. It is also remarkable a maximum mean RMSE for the speed at 0.58 kt and around 70 kg for the aircraft mass (and below 1 kg for the climb profiles). Overall, such results show the validity of the IMM-based method for both aircraft state estimation and GM identification. But to further support the discussion, we get into each VT specificity.

A graphical representation of the GM identification performance is shown in Fig. 3, with the results given with respect to along-path distance. This allows to clearly distinguish the different phases of the VTs and how the different GM change (depicting as well clean or non-clean configuration settings). For each VT, the upper subplot shows the true GM; the middle subplot gives the estimated GM, that is, the one with maximum probability at each time step; and the lower subplot shows the different mode probabilities as given by the filter.

- First, notice the good results obtained for VT3 (Fig. 3c) and VT4 (Fig. 3d), a typical descent and climb, respectively, for which the EKF-IMM is able to correctly identify the active mode with almost no identification delay. The same for the low altitude climb in VT6 (Fig. 3f), where the EKF-IMM is again able to correctly identify all the GM with a very low identification delay.
- Regarding the early descent VT1 (Fig. 3a), the EKF-IMM perfectly identifies all the phases except the fourth phase, where the aircraft is flying in `VS-CAS` with high-lift devices retracted. Notice that in this phase the estimated GM mainly jumps between `VS-CAS-clean` and `VS-CAS-non-clean`, which have almost the same probability, that is, those two modes are not sufficiently distinct for the IMM. Even if such ambiguity increases the identification error, the true GM is correctly identified if we disregard the configuration of the high-lift device. These jumps also influence the state estimation accuracy. Note that this is not a problem in practice because this phase comes just after the cruise phase, therefore it is extremely unlikely that the aircraft deploys flaps/slats at such altitude and speed, indeed leading to a correct result.
- The results for VT2 (Fig. 3b) are similar to those for VT1, that is, all phases are perfectly identified except for one, in this case, the first one. Again, the guidance mode probability mainly jumps between `FPA-CAS-clean` and `FPA-CAS-non-clean`, which are not sufficiently distinct for the IMM to correctly estimate the mode.
- The most challenging trajectory is VT5, shown in (Fig. 3e). This VT was selected to show the limitations of the EKF-IMM approach proposed in this article. First, notice that the algorithm is able to correctly identify the last two phases (phase 8 and 7) with clean configurations (i.e., `CAS-THR` and `DEC-THR`). But for the subsequent phases,

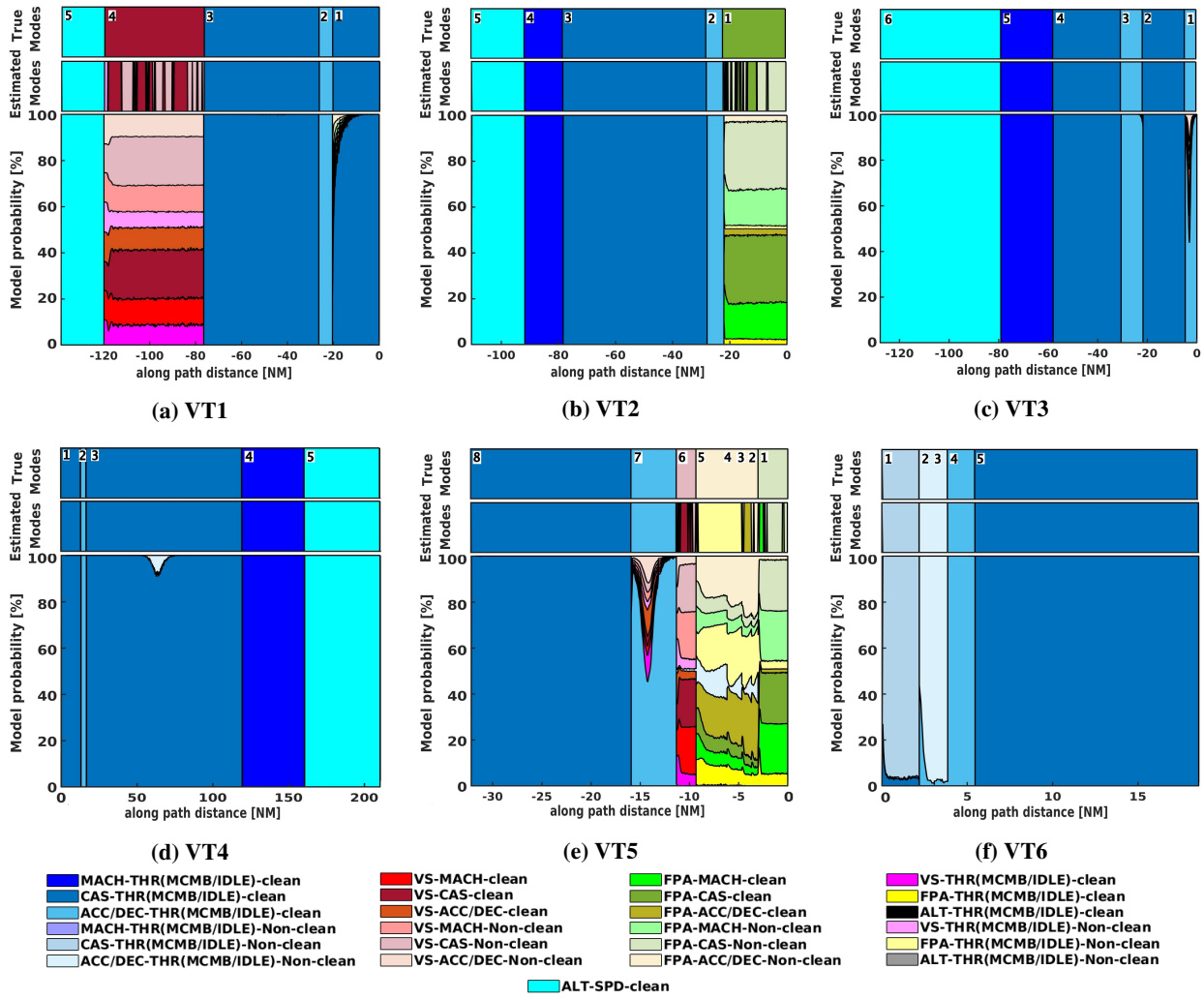

Fig. 3 For each simulated VT: (upper subplot) true GM, (middle subplot) estimated GM, and (lower subplot) IMM-based mode probabilities. GM colour code at the bottom of the figure.

where the aircraft is flying at `VS-CAS`, `FPA-DEC` and `FPA-CAS`, with different configuration settings, several identification ambiguities appear. In the sixth phase (`VS-CAS`) the IMM assigns almost equal probability to four modes: `VS-MACH-clean`, `VS-CAS-clean`, `VS-MACH-non-clean` and `VS-CAS-non-clean`. At the end, these modes are very similar, and being able to identify the first command is already valuable. The same happens for the following phases, for instance in the first one, where the IMM assigns almost equal probability to four modes: `FPA-MACH-clean`, `FPA-CAS-clean`, `FPA-MACH-non-clean`, and `FPA-CAS-non-clean`. Although these four modes at lower altitudes are very similar in terms of kinetic and potential energy rates, the constant FPA outcome is correct. In conclusion, even in such challenging scenario, the IMM-based solution behaves well, but for some of the modes the configuration setting is not identifiable.

V. Results with Real Data

A set of FDR data of a narrow-body jet aircraft from a European airline is taken to further validate the proposed method. Measurements can be obtained from secondary surveillance radars to feed the proposed filtering technique. Some companies (e.g., OpenSky [44], flightradar24, and FlightAware) provide secondary surveillance radar data, mostly ADS-B, but with some limitations. For instance, secondary surveillance radars do not have a worldwide coverage, or some of this data was not available in the past; for OpenSky, only data after 2013 is available. Airlines policy toward not sharing FDR data adds to the challenge of real data accessibility.

For this study, some challenges had to be addressed: i) the data set did not contain the (true) GM, which is the object of estimation by our application; ii) the measurements (i.e., ADS-B and EHS data) associated with the available FDR were not obtainable either; iii) a known parameters vector is required for each mode to compute the control vector; and iv) the atmospheric and weather conditions (non-ISA model) of the flights recorded in the FDR had to be taken into account. Fig. 4 shows the setup to address these challenges:

- To address the first challenge, some close data inspection/processing was needed to guess the true GM executed by the aircraft from the available FDR.
- Regarding ADS-B and EHS data: while ADS-B is automatically transmitted by the aircraft at a given frequency rate, EHS information is replied to the ATC system who initiated the interrogation [39]. Thus, the ADS-B and EHS data are broadcast by the airplane itself, and the same information is stored in the FDR, then being able to build the measurement vector. For this work, it was not possible to obtain the ADS-B data that was broadcast by the aircraft available in the FDR data set. Thus, the ADS-B information used in this validation has been synthesized from the FDR dataset. We assume that the potential differences between the broadcast parameters through ADS-B and the recorded counterpart in the FDR is not noticeable.
- The FDR data available was also analyzed to obtain the corresponding parameters $\mathbf{p}$, to compute the control $\mathbf{u}$.
- To address the last challenge, historical re-analysis weather data from the European Centre for Medium-Range Weather Forecasts (ECMWF) was used to provide the weather and atmospheric conditions for the particular FDR flight under analysis. ECMWF website provides reanalysis and weather forecast data. Reanalyzed data is obtained from the reassessment of the forecast model according to its counterparts' archived observations (i.e., historical model). The true state vector (i.e., ground truth) is generated by extracting pressure altitude, along-path distance, and aircraft mass directly from the FDR data set. Notice that FDR contains ground speed, while true airspeed—a state variable—is computed through the effect of the wind—available from ECMWF—on the ground speed. Moreover, atmospheric conditions—temperature and pressure variables—of the true state vector are also acquired from ECMWF.

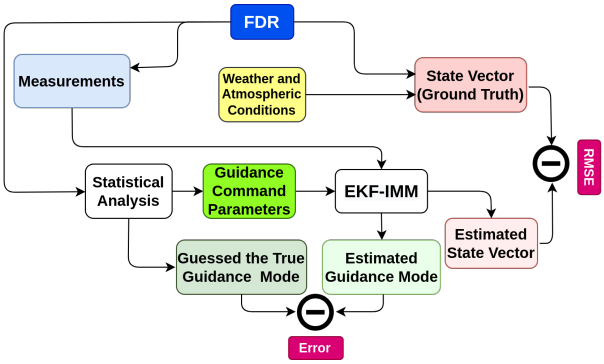

Fig. 4 Setup for the real-time processing of real data.

A. Real validation trajectories selected

Two flights were considered, representative of a typical climb and a descent vertical trajectory profiles (the aircraft type for both real flights were the same, i.e., a narrow-body jet aircraft). This allows to i) further validate the proposed methodology, with respect to the synthetic data scenarios, and ii) find the limitations of this methodology in non-nominal real-life scenarios. Tables 9 and 10 describe the real validation trajectories 1 and 2 (RVT1 and RVT2). Notice that while guidance command parameters were known in the validation done in Sec. IV, using real data the parameters are obtained from the measurements.

Table 9 RVT1: climb trajectory profile

Phase	GM	Command1	Command2	End Condition	Configuration
1	CAS-THR	$\bar{v}_{\text{CAS}} = 280\,\text{kt}$	$\bar{\pi} = 1$	$M = 0.76$	CLEAN-UP
2	MACH-THR	$\bar{M} = 0.76$	$\bar{\pi} = 1$	$v_{\text{CAS}} = 255\,\text{kt}$	CLEAN-UP
3	VS-THR	$\bar{v}_h = 1050\,\text{ft/min}$	$\bar{\pi} = 1$	$v_{\text{CAS}} = 245\,\text{kt}$	CLEAN-UP
4	VS-CAS	$\bar{v}_h = 1050\,\text{ft/min}$	$\bar{v}_{\text{CAS}} = 245\,\text{kt}$	$h_p = \text{FL374}$	CLEAN-UP
5	VS-THR	$\bar{v}_h = 1050\,\text{ft/min}$	$\bar{\pi} = 1$	$h_p = \text{FL380}$	CLEAN-UP
6	ALT-MACH	$\bar{v}_h = 0$ ($h_p = \text{FL380}$)	$\bar{M} = 0.77$	$\Delta s = 25\,\text{NM}$	CLEAN-UP

Table 10 RVT2: Descent trajectory profile

Phase	GM	Command1	Command2	End Condition	Configuration
1	ALT-MACH	$\bar{v}_h = 0$ ($h_p = \text{FL320}$)	$\bar{M} = 0.747$	$\Delta s = 10\,\text{NM}$	CLEAN-UP
2	CAS-THR	$\bar{v}_{\text{CAS}} = 270\,\text{kt}$	$\bar{\pi} = 0$	$h_p = \text{FL104.8}$	CLEAN-UP
3	DEC-THR	$\bar{k}_{esf} = 0.3$	$\bar{\pi} = 0$	$v_{\text{CAS}} = 250\,\text{kt}$	CLEAN-UP
4	CAS-THR	$\bar{v}_{\text{CAS}} = 250\,\text{kt}$	$\bar{\pi} = 0$	$h_p = 5712\,\text{ft}$	CLEAN-UP
5	FPA-CAS	$\bar{\gamma}_g = -2.15\,\text{deg}$	$\bar{v}_{\text{CAS}} = 250\,\text{kt}$	$h_p = 2560\,\text{ft}$	CLEAN-UP

The climb trajectory (RVT1) starts at $h_p = \text{FL200}$ until reaching $\bar{M} = 0.76$ in a constant calibrated airspeed

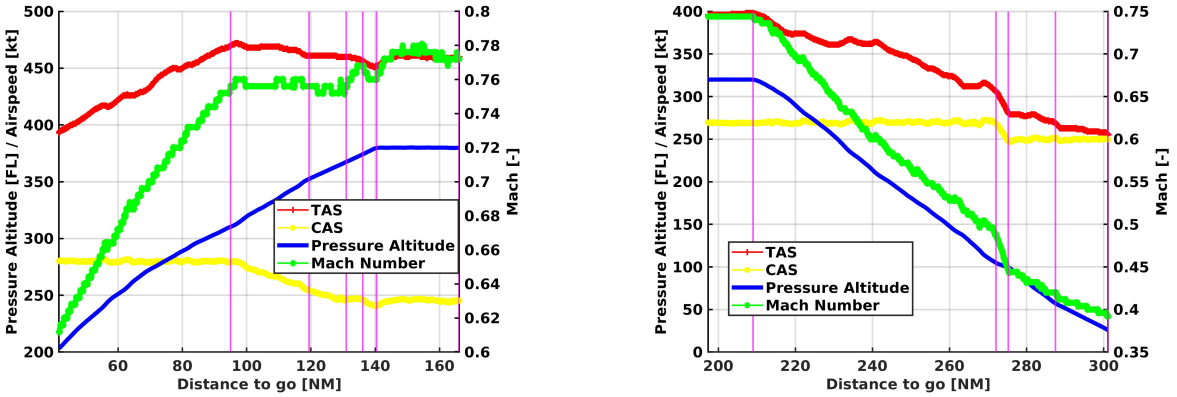

(a) RVT1 **(b) RVT2**

Fig. 5 Real trajectories from FDR data.

$\bar{v}_{\text{CAS}} = 280\,\text{kt}$ and maximum throttle rate mode (`CAS-THR`). Afterwards, the aircraft flies at a constant Mach number and the thrust is kept at the maximum possible rate (`MACH-THR`) until reaching $\bar{v}_{\text{CAS}} = 255\,\text{kt}$. Then, the pilot changes the mode to fly at a constant vertical speed $\bar{v}_h = 1050\,\text{ft/min}$ with maximum thrust (`VS-THR`) to reduce the calibrated airspeed value until $\bar{v}_{\text{CAS}} = 245\,\text{kt}$. Then, a constant vertical speed and a constant calibrated airspeed are kept (`VS-CAS`) until FL374. The last section of the climb involves flying at a constant vertical speed with maximum thrust mode (`VS-THR`) to reach the cruise phase at FL380. Finally, the cruise phase (`ALT-SPD`) lasts for a distance of 25NM (i.e., $\Delta s = 25\,\text{NM}$).

The descent profile (RVT2) begins with a cruise phase at h_p = FL320, where speed is constant ($\bar{v}_{\text{CAS}} = 270\,\text{kt}$ and $\bar{M} = 0.747$). The top of descent (TOD) is located at a distance $\Delta s = 10\,\text{NM}$. After the TOD, the throttle is set to the minimum rate, which leads to an idle-thrust and constant calibrated airspeed $\bar{v}_{\text{CAS}} = 270\,\text{kt}$ (`CAS-THR`) descent until FL104.8. Afterwards, the calibrated airspeed is reduced to $\bar{v}_{\text{CAS}} = 250\,\text{kt}$ by flying a `DEC-THR` mode. This constant calibrated airspeed ($\bar{v}_{\text{CAS}} = 250\,\text{kt}$) is kept for the last two modes: in the first one, the throttle is fixed at the minimum rate (`CAS-THR`) to reach $h_p = 5712\,\text{ft}$; in the second one, the aircraft flies with a constant FPA (`FPA-CAS`) to reach $h_p = 2560\,\text{ft}$. In addition, high-lift devices are retracted in these two real profiles, which leads to clean configurations.

Fig. 5a and 5b show these trajectory profiles. Notice that compared to the synthetic trajectories of Sec. IV (VT1-6), these real trajectories present much more noisy profiles (i.e., clean dynamics are not available, and noisy measurements are used), which has an impact on the filter performance.

B. Results

It is important to notice, as previously stated, that the exact aircraft motion model and the performance model that are used in the FMSs are unknown. Besides, the weather models in the FMSs are very simple, only including wind information for a few (3-5) different altitudes. Therefore, such model mismatch and weather/atmospheric uncertainties,

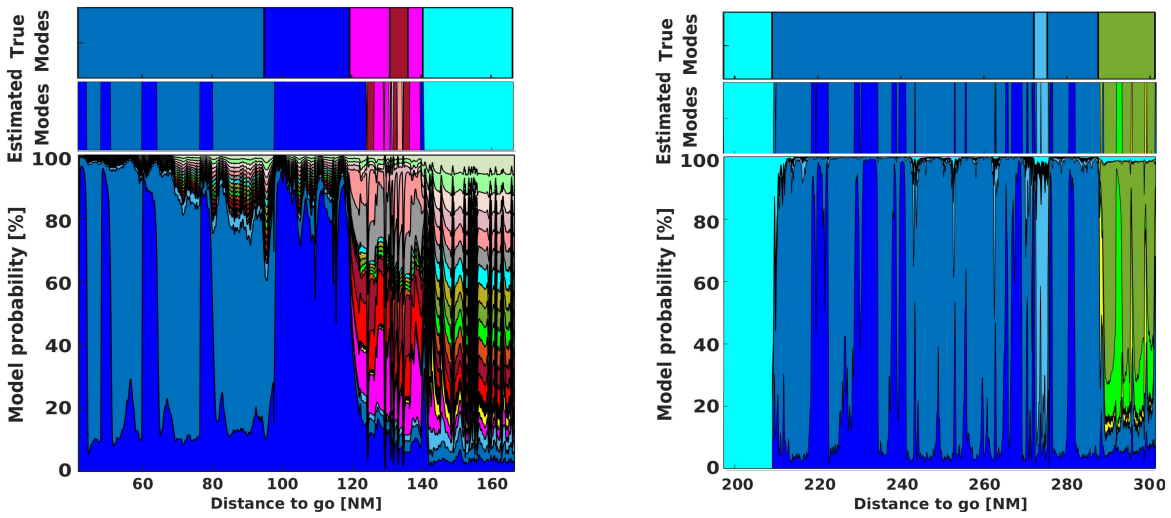

(a) RVT1 (b) RVT2

Fig. 6 For both real VTs: the guessed true GM (upper subplot), estimated GM (middle subplot), and IMM-based mode probabilities (lower subplot).

impact the trajectory estimation/prediction and the guidance mode identification in real-life applications, with respect to the nominal synthetic data case, as shown hereafter.

The results are shown in Fig. 6a and 6b. Regarding RVT1, the initial climb mode (`CAS-THR`) is affected by the noisy Mach number (which was not the case for the synthetic VTs). Indeed, the probability of constant Mach number is higher than flying at a constant calibrated airspeed in some short portions of this guidance mode, consequently, the EKF-IMM identifies `MACH-THR`. Therefore, one of the two commands is not always correctly identified. The second mode is clearly identified with a short delay. This is because a moving average filter was applied to the calibrated airspeed and Mach number in order to reduce the effects of dealing with noisy FDR data. In the third and fifth modes (`VS-THR`), the noisy Mach number induces again a misidentification leading to an estimated `MACH-THR` mode in some short portions. This implies that only one of the two commands is not correct all the time. In some portions of the fourth mode (`VS-CAS`), the configuration setting is not correctly identified. Still, in such high altitudes and for the type of operations considered in this article, high-lift devices are always retracted. Therefore, the fact that the EKF-IMM cannot correctly identify the mode is considered of negligible significance.

In the cruise phase, altitude, speed, and FPA are constant, which leads to identify several guidance modes with a close probability. Considering the summation of these probabilities leads to the correct `ALT-SPD` mode identification. Notice that the overall performance is reasonably good, but extracting the data from the FDR to build the scenario reduces the accuracy of the estimated active guidance modes.

The results for RVT2 show the same impact of the noisy FDR data. Again, the different guidance modes are correctly identified almost all the time, with some short misidentifications induced by such noisy FDR data. Finally, Table 11

shows the mean RMSE for each state variable, showing again a good performance of the EKF-IMM filter. It is worth noting that the aircraft motion model in (1) is generic, nevertheless, the wind has been neglected for our case studies. As shown in (1), the weather model affects the accuracy of the along-path distance variable (s) in the EKF-IMM filtering method. Table 11 shows a relatively larger estimation error for this state variable in all validation trajectories.

Table 11 Error in the real climb and descent profiles.

	RMSE_h	RMSE_s	RMSE_v	RMSE_m	RMSE_τ	RMSE_p
Climb	0.026 ft	3.58 NM	1.04 kt	536.2 kg	1.14 K	136.56 Pa
Descent	8.01 ft	1.97 NM	11.28 kt	55.82 kg	0.31 K	226.29 Pa

Overall, we can still say that the IMM-based GM identification approach is a promising solution, given that even with real (and noisy) FDR data the filter is able to identify the correct modes almost all the time. This real data analysis completes the statistical characterization conducted with synthetic data (i.e., ground truth-like, ADS-B and EHS-like simulated trajectories) described in Sec. IV, and shows that in real-life applications the uncertainty of both the weather and parameters vector must be taken into account.

VI. Conclusion

Although aircraft trajectories are planned through aircraft intents, some guidance commands may change during the flight to cope with execution uncertainty. Hence, aircraft intent uncertainty may impact the trajectory prediction (TP) performance, a problem that can be mitigated with the identification of these guidance modes. It is worth noting that the proposed estimation method relies only on surveillance data broadcast by the target aircraft. Then, this could be part of a ground-based air traffic management (ATM) tool, but also on-board the aircraft to allow self-separation or conformance monitoring capabilities.

An IMM-based filter is proposed to identify the active guidance mode among all possible command pairs. Several validation trajectories are considered to perform a statistically meaningful optimal EKF-IMM analysis in representative scenarios. The aim of such analysis is to obtain the nominal baseline performance of the proposed approach, providing a benchmark for the design of methods for real-life conditions. The performance of the proposed approach is clear from the results obtained, where in clean configurations, the active guidance mode can be unambiguously identified in climb/descent flight phases. The limitations of the method were also shown through a low-altitude descent, with different non-clean configurations (i.e., flaps/slats and landing gear). In such cases, the filter is not always able to identify the correct mode but still can provide some meaningful information.

The statistical characterization of the filter under nominal conditions is further completed with two real scenarios. Again, even with the FDR data limitations to construct the test setup, it is shown that the filter can still provide a good

performance. However, in such real trajectories, the full set of uncertainties should be considered in order to potentially obtain close-to-optimal solutions.

This paper focused on optimal guidance mode identification (i.e., under nominal conditions), which opens the door to several future works: i) performance under more realistic conditions (e.g., model mismatch and weather uncertainty); ii) estimation of the initial mass of the aircraft; iii) correct identification of the high-lift devices position; iv) robust filter design and sensitivity analysis under model mismatch or system uncertainties; v) new solutions for multi-aircraft and cooperative scenarios; or vi) the generalization to more advanced Bayesian filtering techniques such as particle filters.

A. Appendix: Control Vector Computation for the Set of Guidance Modes

This appendix gives the mathematical details to obtain the control vector $\mathbf{u} = [\gamma, \pi]^\top$, for each pair of guidance commands identified in Table 1.

A. Energy share factor

First, define the energy share factor k_{esf} as a variable that relates how much of the available power is allocated to gain the potential energy in climb or descent,

$$k_{esf} = \left(1 + \frac{v}{g}\frac{\mathrm{d}v}{\mathrm{d}h}\right)^{-1}, \tag{13}$$

with v is the true airspeed; h the geometric altitude; and g the gravity acceleration. If the aircraft is climbing or descending at constant Mach ($\bar{M}$), the corresponding energy share factor can be computed combining (13) and (4). In ISA, this yields to

$$k_{esf}|_{\dot{M}=0} = \begin{cases} (1 - \frac{\lambda_\tau R \gamma_a}{2g}\bar{M}^2)^{-1} & \text{if } h \leq h_t \\ 1 & \text{if } h > h_t \end{cases}, \tag{14}$$

where λ_τ is the temperature lapse rate (i.e. the partial derivative of the temperature with respect to the altitude according to the ISA model); R is the ideal gas constant of the air; γ_a is the specific heat ratio of the air; $\bar{M}$ stands for a constant Mach number; and $h_t = 11\,\mathrm{km}$ (above the mean sea level) is the tropopause altitude. Similarly, combining (13) and (5), and assuming ISA conditions, the energy share factor for a climb/descent flown at a given constant calibrated airspeed ($\bar{v}_{\mathrm{CAS}}$) is

$$k_{esf}|_{\dot{v}_{\mathrm{CAS}}=0} = \begin{cases} (B(\bar{v}_{\mathrm{CAS}}, h_p) - C(\bar{v}_{\mathrm{CAS}}, h_p))^{-1} & \text{if } h \leq h_t \\ (B(\bar{v}_{\mathrm{CAS}}, h_p)^{-1} & \text{if } h > h_t \end{cases} \tag{15}$$

with

$$A(\bar{v}_{\mathrm{CAS}}) = (1 + \bar{v}_{\mathrm{CAS}}^2 \frac{\mu\rho_0}{2p_0})^{\frac{1}{\mu}} - 1$$

$$B(\bar{v}_{\mathrm{CAS}}, h_p) = 1 + \frac{A(\bar{v}_{\mathrm{CAS}})}{\delta(h_p)}\left(\frac{A(\bar{v}_{\mathrm{CAS}})}{\delta(h_p)} + 1\right)^{\mu-1}$$

$$C(\bar{v}_{\mathrm{CAS}}, h_p) = R\frac{\lambda_\tau}{\mu g}\left[\left(\frac{A(\bar{v}_{\mathrm{CAS}})}{\delta(h_p)} + 1\right)^{\mu} - 1\right]$$

where $\mu = (\gamma_a - 1)\gamma_a^{-1}$; ρ_0 and p_0 are the standard density and pressure values at the sea level; δ is the normalized air pressure, which depends on the pressure altitude (h_p); and $\bar{v}_{\mathrm{CAS}}$ stands for the constant calibrated airspeed.

These equations could also be obtained in non-ISA conditions, providing that a differentiable model for temperature and pressure is given. The energy share factor will be used hereafter to simplify the notation of certain mathematical expressions, but also because it is a parameter for acceleration/deceleration commands in Table 1.

B. Speed and throttle modes

The first set of guidance pairs in Table 1 command a fixed throttle setting in Command 2. Command 1 is commanding either a constant Mach, calibrated airspeed or acceleration/deceleration. Combining (1) and (13) we obtain

$$\gamma = \arcsin\left(\frac{T - D}{mg} k_{esf}\right), \tag{16}$$

with T the total thrust (fixed $\bar{\pi}$), D the aerodynamic drag, and m the aircraft mass. For `ACC/DEC` guidance commands, the energy share factor k_{esf} is directly specified by the guidance system. For `MACH` and `CAS`, k_{esf} is given by (14) and (15).

C. Vertical speed and speed modes

The second set of guidance pairs in Table 1 command the elevator (Command 1) to keep a fixed vertical speed ($\bar{v}_h$), while the throttle (Command 2) is then adjusted to maintain a certain speed or a certain acceleration/deceleration. Assuming ISA conditions $v_h = \dot{h}$ and using (1), the aerodynamic FPA can be obtained as

$$\gamma = \arcsin\left(\frac{\bar{v}_h}{v}\right). \tag{17}$$

In non-ISA conditions, the vertical speed could be expressed as the derivative of the pressure altitude, providing that a differentiable model for temperature and pressure is given. Once the FPA is computed, the throttle required to command a certain speed or acceleration/deceleration is

$$\pi = \frac{D + k_{esf}^{-1} mg \sin\gamma - T_{\mathrm{idle}}}{T_{\max} - T_{\mathrm{idle}}}, \tag{18}$$

where $T_{\max}$ and T_{idle} are the maximum and minimum thrust values (i.e., maximum/minimum throttle rate is deployed).

D. Ground FPA and speed modes

The third set of guidance pairs in table 1 command the elevator (Command 1) to keep a fixed ground FPA ($\bar{\gamma}_g$), while the throttle (Command 2) is then adjusted to maintain a certain speed or acceleration/deceleration. The ground FPA and the aerodynamic FPA (γ) are related with the wind as follows (neglecting any vertical wind component):

$$\gamma = \arcsin(\sin\bar{\gamma}_g(\sqrt{1-\overline{W}_x^2-\overline{W}_s^2\sin^2\bar{\gamma}_g}+\overline{W}_s\cos\bar{\gamma}_g)), \tag{19}$$

where $\overline{W}_s = W_s/v$ and $\overline{W}_x = W_x/v$ are the normalized wind components (along-path and crosswind). Again, once the FPA is computed, the throttle required to command a certain speed or acceleration/deceleration is given by (18).

E. Vertical path and throttle modes

The fourth set of guidance pairs in Table 1 command the elevator (Command 1) to follow a specific vertical trajectory profile (either at constant vertical speed, constant ground FPA, or constant altitude), while a fixed throttle setting is given for Command 2. Then, the total thrust T can be obtained with a fixed $\bar{\pi}$, and the FPA can be derived from (1). For the `VS` command, the FPA is given by (17), for the `FPA` command it is given by (19), while for `ALT` the FPA is zero (if neglecting the air pressure variations along the flight for a given altitude).

F. Altitude-speed mode

If we assume that the partial derivative of the air pressure as a function of the distance flown is zero, the aerodynamic FPA is zero and the required throttle, as seen from (1), is such that thrust equals aerodynamic drag, i.e.,

$$\pi = \frac{D - T_{\text{idle}}}{T_{\max} - T_{\text{idle}}}. \tag{20}$$

Since the pressure altitude is constant, following a constant `Mach` is equivalent to follow a constant `CAS`. Thus, this mode could accept either a target `Mach` or target `CAS` as guidance (known) parameter. Recall that the aerodynamic drag (D) and also the idle and maximum thrust magnitudes depend, in general, on the aircraft speed.

Funding Sources

This work has been partially supported by a EU ENGAGE KTN PhD Fellowship, and the DGA/AID project 2022.65.0082.

Table 12 Symbol and parameters

Symbol	Parameter	Symbol	Parameter
$\mathbf{x}$	state vector	$\mathbf{y}$	measurement vector
h	geometric height	s	Distance
v	true airspeed	m	aircraft mass
τ	temperature	p	pressure
T	total thrust	D	aerodynamic drag
γ	aerodynamic FPA	π	engine throttle
q	total fuel flow	ξ	HLiD setting
W_x	crosswind	W_s	head (tail) wind
g	gravity acceleration	T_{idle}	residual thrust
T_{max}	maximum thrust	c_i	ith path constraint
$\mathbf{u}$	control vector	$\mathbf{p}$	known command parameters
M	Mach number	v_{CAS}	Calibrated airspeed
γ_a	heat ratio of the air	R	perfect gas constant
ρ_0	standard air density	p_0	standard pressure
μ	constant	$\bar{W}_s$	normalized head/tail wind
$\bar{W}_x$	normalized crosswind	$\bar{M}$	Mach as a guidance command parameter
$\bar{v}_{CAS}$	guidance command parameter at constant CAS	$\bar{k}_{esf}$	energy share factor as a guidance parameter
$\bar{v}_h$	vertical speed as a guidance parameter	$\bar{\pi}$	throttle parameter as a guidance parameter
$\bar{\gamma}_g$	ground FPA as a guidance parameter	N	possible GMs considered in this paper
$\mathbf{f}$	process function	$\mathbf{h}$	measurement function
$\mathbf{w}$	process noise	$\mathbf{v}$	measurement noise
h_p	pressure altitude	v_g	ground speed
$\dot{h}$	derivative of geometric height	$\dot{s}$	derivative of distance
$\dot{v}$	derivative of true airspeed	$\dot{m}$	derivative of aircraft mass
$\dot{\tau}$	derivative of temperature	$\dot{p}$	derivative of pressure
$\mathcal{N}$	Gaussian distribution	θ	mode state
$\mathbf{Q}$	process noise covariance	$\mathbf{R}$	measurement noise covariance
μ_k^i	posterior of (ith) mode probability at kth time step	$\hat{x}_{k\|k}^i$	(ith) EKF estimate of state vector at kth time step
$\hat{P}_{k\|k}^i$	(ith) covariance at kth time step	r_{ji}	transition probability elements
Π	transition probability matrix	$\widehat{\mathbf{x}}_{k-1\|k-1}^{0i}$	ith mixed estimated state vector
$\mathbf{P}_{k-1\|k-1}^{0i}$	ith mixed covariance as a filter (EKF) input	$\mu_{k-1\|k-1}^{ji}$	mixing probability
F^i	Jacobian of f^i	H^i	Jacobian of h^i
S^i	innovation covariance matrix associated ith filter	K^i	Kalman gain
$\widehat{x}_{k\|k}$	the final estimation state vector	$P_{k\|k}$	the final estimation error covariance
$\widehat{GM}$	identified GM	ΔS	distance during a given phase
FL	flight level	rho	air density
λ_τ	temperature lapse rate	τ_h	temperature derivative with respect to altitude
p_h	pressure derivative with respect to altitude	$\Delta\tau$	temperature deviation
e_{ident}	erroneous identification	$\dot{M}$	Mach derivative
$\dot{v}_{CAS}$	CAS derivative	h_t	tropopause altitude

References

[1] Brooker, P., "SESAR and NextGen: Investing in new paradigms," The Journal of Navigation, Vol. 61, No. 2, 2008, p. 195. https://doi.org/https://doi.org/10.1017/S0373463307004596.

[2] SESAR Joint Undertaking, "European ATM Master Plan. Digitalising Europe's aviation infrastructure," Tech. rep., 2019. Executive view.

[3] Duan, P. P., Uijt de Haag, M., and Etherington, T., "Energy state prediction methods for airplane state awareness," Proc. of the IEEE/AIAA Digital Avionics Systems Conference, 2016. https://doi.org/http://dx.doi.org/10.1109/DASC.2016.7778085.

[4] Noskievič, T., and Kraus, J., "Air traffic control tools assessment," MAD-Magazine of Aviation Development, Vol. 5, No. 2, 2017, pp. 6–10. https://doi.org/https://doi.org/10.14311/MAD.2017.02.01.

[5] Schuster, W., and Ochieng, W., "Performance requirements of future Trajectory Prediction and Conflict Detection and Resolution tools within SESAR and NextGen: Framework for the derivation and discussion," Journal of Air Transport Management, Vol. 35, 2014, pp. 92–101. https://doi.org/https://doi.org/10.1016/j.jairtraman.2013.11.005.

[6] Tang, J., "Conflict detection and resolution for civil aviation: A literature survey," IEEE Aerosp. Electron. Syst. Mag., Vol. 34, 2019, pp. 20–35. https://doi.org/http://dx.doi.org/10.1109/MAES.2019.2914986.

[7] Legrand, K., Rabut, C., and Delahaye, D., "Wind networking applied to aircraft trajectory prediction," Proc. of the IEEE/AIAA Digital Avionics Systems Conference, 2015. https://doi.org/http://dx.doi.org/10.1109/DASC.2015.7311330.

[8] Casado Magaña, E. J., "Trajectory prediction uncertainty modelling for Air Traffic Management," Ph.D. thesis, University of Glasgow, Glasgow, UK, 2016.

[9] Lopez Leones, J., "Definition of an aircraft intent description language for air traffic management applications," Ph.D. thesis, University of Glasgow, 2008.

[10] Casado, E., D'Alto, L., and Vilaplana, M., "Analysis of the impact of intent uncertainty on the accuracy of predicted trajectories for arrival management automation," 6th International Conference on Research in Air Transportation, 2014.

[11] Georgiou, H., Karagiorgou, S., Kontoulis, Y., Pelekis, N., Petrou, P., Scarlatti, D., and Theodoridis, Y., "Moving Object Analytics: Survey on Future Location & Trajectory Prediction Methods," Tech. rep., 2018.

[12] Wang, Z., Liang, M., and Delahaye, D., "A Hybrid Machine Learning Model for Short-term Estimated Time of Arrival Prediction in Terminal Manoeuvring Area," Transportation Research Part C: Emerging Technologies, Vol. 95, 2018, pp. 280–294. https://doi.org/http://dx.doi.org/10.1016/j.trc.2018.07.019.

[13] Jarry, G., Delahaye, D., and Feron, E., "Approach and landing aircraft on-board parameters estimation with LSTM networks," International Conference on Artificial Intelligence and Data Analytics for Air Transportation (AIDA-AT), 2020.

[14] Jarry, G., Delahaye, D., Nicol, F., and Féron, E., "Aircraft atypical approach detection using functional principal component analysis," Journal of Air Transport Management, Vol. 84, 2020.

[15] ICAO, D., "9871: Technical Provisions for Mode S Services and Extended Squitter, AN/464," 2008.

[16] Grappel, R. D., Harris, G. S., Kozar, M. J., and Wiken, R. T., "Elementary surveillance (ELS) and enhanced surveillance (EHS) validation via mode S secondary radar surveillance," Project Report ATC-337, Lincoln Lab., MIT, 2008.

[17] RTCA, Minimum Operational Performance Standards (MOPS) for 1090 MHz Extended Squitter Automatic Dependent Surveillance-Broadcast (ADS-B) and Traffic Information Services-Broadcast (TIS-B), RTCA, Incorporated, 2011.

[18] Guerreiro, N. M., and Underwood, M. C., "Understanding Extended Projected Profile (EPP) Trajectory Error Using a Medium-Fidelity Aircraft Simulation," Aviation Technology, Integration, and Operations Conference, 2018. https://doi.org/http://dx.doi.org/10.2514/6.2018-3044.

[19] Bronsvoort, J., McDonald, G., Paglione, M., Young, C. M., Boucquey, J., Hochwarth, J. K., and Gallo, E., "Real-time trajectory predictor calibration through extended projected profile down-link," USA/Europe Air Traffic Management Research and Development Seminar, 2015.

[20] Weitz, P., "Determination and visualization of uncertainties in 4D-trajectory prediction," 2013 Integrated Communications, Navigation and Surveillance Conference (ICNS), IEEE, 2013. https://doi.org/http://dx.doi.org/10.1109/ICNSurv.2013.6548525.

[21] Thipphavong, D. P., Schultz, C. A., Lee, A. G., and Chan, S. H., "Adaptive Algorithm to Improve Trajectory Prediction Accuracy of Climbing Aircraft," Journal of Guidance, Control, and Dynamics, Vol. 36, No. 1, 2013, pp. 15–24. https://doi.org/http://dx.doi.org/10.2514/1.58508.

[22] Liu, W., and Hwang, I., "Probabilistic Trajectory Prediction and Conflict Detection for Air Traffic Control," Journal of Guidance, Control, and Dynamics, Vol. 34, No. 6, 2011, pp. 1779–1789. https://doi.org/http://dx.doi.org/10.2514/1.53645.

[23] Li, X. R., and Jilkov, V. P., "Survey of Maneuvering Target Tracking. Part V: Multiple-Model Methods," IEEE Trans. on Aerospace and Elec. Syst., Vol. 41, No. 4, 2005, pp. 1255–1321.

[24] Wang, Q., and Huang, J., "A VB-IMM filter for ADS-B data," Proc. of the International Conference on Signal Processing, 2014. https://doi.org/http://dx.doi.org/10.1109/ICOSP.2014.7015371.

[25] Khadilkar, H., and Balakrishnan, H., "A Multi-Modal Unscented Kalman Filter for Inference of Aircraft Position and Taxi Mode from Surface Surveillance Data," Proceedings of the AIAA Aviation Technology, Integration, and Operations Conference, 2011. https://doi.org/http://dx.doi.org/10.2514/6.2011-7051.

[26] Jeon, D., Eun, Y., Bang, H., and Yeom, C., "Nonlinear Aircraft Tracking Filter Utilizing a Point Mass Flight Dynamics Model," Proceedings of the Institution of Mechanical Engineers, Part G: Journal of Aerospace Engineering, Vol. 227, No. 11, 2013, pp. 1795–1810. https://doi.org/http://dx.doi.org/10.1177/0954410012463641.

[27] Hwang, I., Hwang, J., and Tomlin, C., "Flight-mode-based Aircraft Conflict Detection using a Residual-mean Interacting Multiple Model Algorithm," Proc. of the AIAA Guidance, Navigation and Control Conference and Exhibit, 2003. https://doi.org/http://dx.doi.org/10.2514/6.2003-5340.

[28] Yepes, J. L., Hwang, I., and Rotea, M., "New Algorithms for Aircraft Intent Inference and Trajectory Prediction," Journal of Guidance, Control and Dynamics, Vol. 30, No. 2, 2007, pp. 370–382. https://doi.org/http://dx.doi.org/10.2514/1.26750.

[29] Dalmau, R., Pérez-Batlle, M., and Prats, X., "Real-time Identification of Guidance Modes in Aircraft Descents Using Surveillace Data," Proc. of the IEEE/AIAA Digital Avionics Systems Conference, 2018. https://doi.org/http://dx.doi.org/10.1109/DASC.2018.8569811.

[30] Blom, H. A., and Bar-Shalom, Y., "The interacting multiple model algorithm for systems with Markovian switching coefficients," IEEE transactions on Automatic Control, Vol. 33, No. 8, 1988, pp. 780–783. https://doi.org/http://dx.doi.org/10.1109/9.1299.

[31] Bronsvoort, J., "Contributions to Trajectory Prediction Theory and its Application to Arrival Management for Air Traffic Control," Ph.D. thesis, Technical University of Madrid (UPM), Madrid, Spain, 2014.

[32] AIRBUS, "Flight Crew Operating Manual, A318/A319/A320/A321, Auto Flight System," Vol. 1, 2005.

[33] AIRBUS, "Flight Crew Operating Manual, A318/A319/A320/A321, FMGS Principles," Vol. 4, 2005.

[34] Hull, D. G., et al., Fundamentals of airplane flight mechanics, Vol. 19, Springer, 2007.

[35] Dalmau, R., "Optimal Trajectory Management for Aircraft Descent Operations Subject to Time Constraints." Ph.D. thesis, Technical University of Catalonia (UPC), Barcelona, Spain, 2019.

[36] Gillet, S., Nuic, A., and Mouillet, V., "Enhancement in realism of ATC simulations by improving aircraft behaviour models," 29th Digital Avionics Systems Conference, IEEE, 2010, pp. 2–D.

[37] Lopez-Leones, J., Vilaplana, A. M., Gallo, E., Navarro, F. A., and Qerejeta, C., "The Aircraft Intent Description Language: A key enabler for air-ground synchronization in Trajectory-Based Operations," Proc. of the IEEE/AIAA Digital Avionics Systems Conference, 2007. https://doi.org/http://dx.doi.org/10.1109/DASC.2007.4391836.

[38] Dalmau, R., Sun, J., and Prats, X., "Fuel Inefficiency Characterisation and Assessment due to Early Execution of Top of Descents. A Case Study for Amsterdam-Schiphol Terminal Airspace using ADS-B data," Proceedings of the 14th USA/Europe Air Traffic Management Research and Development Seminar (ATM2021), 2021.

[39] Sun, J., "Open Aircraft Performance Modeling: Based on an Analysis of Aircraft Surveillance Data." Ph.D. thesis, Delft University of Technology (TUDelft), Delft, Netherlands, 2019.

[40] Blom, H. A. P., and Bloem, E. A., "Exact Bayesian and Particle Filtering of Stochastic Hybrid Systems," IEEE Transactions on Aerospace and Electronic Systems, Vol. 43, No. 1, 2007, pp. 55–70. https://doi.org/http://dx.doi.org/10.1109/TAES.2007.357154.

[41] Arasaratnam, I., Haykin, S., and Elliot, R. J., "Discrete-time Nonlinear Filtering Algorithms using Gauss-Hermite Quadrature," Proc. of the IEEE, Vol. 95, No. 5, 2007, pp. 953–977. https://doi.org/http://dx.doi.org/10.1109/JPROC.2007.894705.

[42] Arasaratnam, I., and Haykin, S., "Cubature Kalman Filters," IEEE Trans. Automatic Control, Vol. 54, No. 6, 2009, pp. 1254–1269.

[43] Eurocontrol, "User manual for the base of aircraft data (BADA). Revision 4.1," Tech. rep., Eurocontrol, Bretigny, France, 2014.

[44] The OpenSky Network, "OpenSky Network," https://opensky-network.org, 2019. Accessed: August 15, 2021.